Research Square

Preprints are preliminary reports that have not undergone peer review.
They should not be considered conclusive, used to inform clinical practice,
or referenced by the media as validated information.

Yin/Yang associated differential responses to Psoralea corylifolia Linn. in rat models: an integrated metabolomics and transcriptomics study

Ming-Liang Zhang
The First Affiliated Hospital of Henan University of Traditional Chinese Medicine
Xu Zhao
5th Medical Center of Chinese PLA General Hospital
Wei-Xia Li
The First Affiliated Hospital of Henan University of Traditional Chinese Medicine
Xiao-Yan Wang
The First Affiliated Hospital of Henan University of Traditional Chinese Medicine
Ming Niu
5th Medical Center of Chinese PLA General Hospital
Hui Zhang
The First Affiliated Hospital of Henan University of Traditional Chinese Medicine
Yu-Long Chen
Henan University of Chinese Medicine
De-Xin Kong
Henan University of Chinese Medicine
Yuan Gao
Capital Medical University School of Traditional Chinese Medicine
Yu-Ming Guo
5th Medical Center of Chinese PLA General Hospital
Zhao-Fang Bai
5th Medical Center of Chinese PLA General Hospital
Xiao-he Xiao
5th Medical Center of Chinese PLA General Hospital
Yan-Ling Zhao
5th Medical Center of Chinese PLA General Hospital
Jinfa Tang (✉ a0519@163.com)
The First Affiliated Hospital of Henan University of CM

Research Article

Keywords: Psoralea corylifolia Linn., liver injury, predisposed individual, metabolomics, transcriptomics

Posted Date: December 6th, 2022

DOI: https://doi.org/10.21203/rs.3.rs-2301287/v1

License: This work is licensed under a Creative Commons Attribution 4.0 International License. Read Full License

Version of Record: A version of this preprint was published at Chinese Medicine on August 17th, 2023. See the published version at https://doi.org/10.1186/s13020-023-00793-x.

Abstract

Aim

Psoralea corylifolia Linn. (BGZ) is a commonly used traditional Chinese medicine (TCM) for the treatment of kidney-yang deficiency syndrome ($Yang_{syn}$) with good curative effect and security. However, BGZ was also reported to induce liver injury in recent years. According to TCM theory, taking BGZ may induce a series of adverse reactions in patients with kidney-yin deficiency syndrome (Yin_{syn}), which suggests that BGZ-induced liver damage may be related to its unreasonable clinical use. The study aimed to investigate the differential responses to BGZ in $Yang_{syn}$ and Yin_{syn} rat models and identify the corresponding characteristic biomarkers.

Materials and methods

The corresponding animal models of $Yang_{syn}$ and Yin_{syn} were induced by hydrocortisone and thyroxine + reserpine respectively. Body weight, organ index, serum biochemistry, and Hematoxylin and Eosin (HE) staining were used to evaluate the liver toxicity effect of BGZ on rats with $Yang_{syn}$ and Yin_{syn}. Transcriptomics and metabonomics were used to screen the representative biomarkers (including metabolites and differentially expressed genes (DEGs)) changed by BGZ in $Yang_{syn}$ and Yin_{syn} rats, respectively.

Results

The level changes of liver organ index, ALT, and AST suggested that BGZ has liver-protective and liver-damaging effects on $Yang_{syn}$ and Yin_{syn} rats, respectively, and the results also were confirmed by the pathological changes of liver tissue. The results showed that 102 DEGs and 27 metabolites were significantly regulated related to BGZ's protective effect on $Yang_{syn}$, which is mainly associated with the glycerophospholipid metabolism, arachidonic acid metabolism, pantothenate, and CoA biosynthesis pathways. While 28 DEGs and 31 metabolites, related to the pathway of pantothenate and CoA biosynthesis, were significantly regulated for the BGZ-induced liver injury in Yin_{syn}. Furthermore, 4 DEGs (Aldh1b1, Slc25a25, Pim3, Oaf) and 4 metabolites (phosphatidate, phosphatidylcholine, N-Acetylleucine, biliverdin) in the $Yang_{syn}$ group and 1 DEGs (Lgals5) and 1 metabolite (5-amino-1-(5-phospho-D-ribosyl)imidazole-4-carboxylate) in Yin_{syn} group were significantly correlated to the ALT and AST levels of BGZ treated and untreated groups ($ROC \geq 0.9$).

Conclusions

Yin_{syn} and $Yang_{syn}$ are the predisposed syndrome for BGZ to exert liver damage and liver protection respectively, which are mainly related to the regulation of amino acid metabolism, lipid metabolism, energy metabolism, and metabolism of cofactors and vitamins. The results further suggest that attention should be

paid to the selection of predisposed populations when using drugs related to the regulation of energy metabolism, and the Yin_{syn}/$Yang_{syn}$ animal models based on the theory of TCM syndromes may be a feasible method for identifying the susceptible population to receive TCM.

1. Introduction

In recent years, the proportion of drug-induced liver injury (DILI) caused by traditional Chinese herbs and dietary supplements has increased year by year (Hoofnagle and Björnsson, 2019; Shen et al., 2019). This is particularly noticeable for non-toxic traditional Chinese medicine (TCM) such as *Polygonum multiflorum* Thunb. (Zhang et al., 2020) and *Psoralea corylifolia* Linn. (BGZ) (Wang et al., 2020), which have been used for thousands of years in China. This increase is causing great confusion for doctors and patients.

DILI usually involves two factors, the “drug” and the “host” (Chen et al., 2015). For drug factors, Chen et al. constructed a “role-of-two” model (Chen et al., 2013) and modified the version used (Chen et al., 2016). The model enhanced the ability to predict whether a drug will cause DILI, but it was unable to fully explain individual differences in drug usage. Therefore, it cannot be used to predict individuals who are predisposed to DILI. Host factors are also important in understanding the susceptibility to DILI. Host factors that are generally recognized by modern research include hosts who carry specific HLA genes or the immune homeostasis of the host (Chen et al., 2016). This is consistent with the concept of TCM syndrome, which summarizes the pathological changes of the body at a certain stage of disease development based on TCM theory. TCM treatment requires “therapy based on syndrome differentiation.” Symptomatic treatment can result in a better therapeutic effect, otherwise, it can aggravate the disease process and induce new diseases. Therefore, it may be feasible to explore the predisposition of individuals to TCM liver injury based on TCM syndrome theory.

BGZ has been used for many years in China to treat symptoms such as impotence, nocturnal emission, enuresis, frequent urination, cold aching in the lower back and knees, kidney deficiency, and premature ejaculation (Chinese Pharmacopoeia Commission (2020)). BGZ has definite pharmacological effects, such as anti-tumor, anti-oxidation, antibacterial, anti-inflammatory, anti-depression, estrogen level regulation, bone growth promotion, nerve protection, and influence on the liver (Zhang et al., 2016). Its active ingredients, psoralen and 5-methoxypsoralen, have become commonly used in the clinical treatment of vitiligo and psoriasis (Gupta and Anderson, 1987; McNeely and Goa, 1998). In addition, BGZ and its related compounds are also commonly used in health food and dietary supplements. However, in recent years, BGZ and its related compound preparations Zhuanggu Guanjie Pill and Xianling Gubao Capsules were reported to induce DILI in China (Deng et al., 1996, Li et al., 2020; Liu et al., 2019; Wang et al., 2020). The BGZ-induced liver injury also occurred in South Korea (Nam et al., 2005).

Although some studies have confirmed that BGZ and some of its components have hepatotoxicity (Li et al., 2017; Wang et al., 2020; Zhang et al., 2022), these studies only focused on the drug itself and did not consider the host factors that induced DILI. Accordingly, by integrating the basic disease characteristics of the population treated with BGZ, our previous study found that most BGZ-induced DILI patients had osteoporosis, psoriasis, osteoarthritis, and other basic diseases related to immune activation (Ge et al.,

2021), and such diseases were found to be closely related to the imbalance of kidney-yang deficiency syndrome ($Yang_{syn}$) and kidney-yin deficiency syndrome (Yin_{syn}) according to TCM diagnosis (Dermatology Branch of China Association of Chinese Medicine. 2017, Dermatology Branch of China Association of Chinese Medicine. 2018, Ge et al. 2020). The ancient TCM medicine book “Lei Gong Concocting (Paozhi) Theory” also recorded during the Northern and Southern Dynasties in China that people with “asthenic yin causing excessive pyrexia” should avoid taking BGZ. Thus, the BGZ-induced DILI may be related to its inappropriate symptomatic treatment. However, whether it has a causal relationship with the imbalance of $Yang_{syn}$ and Yin_{syn} in the body remains unclear.

Continuously administered high doses of exogenous glucocorticoid (GC) (e.g., hydrocortisone) (Zhang et al., 2019) or thyroxine + reserpine (Wang, P. et al., 2010) in rats results in symptoms similar to $Yang_{syn}$ or Yin_{syn}, respectively, and play important roles in the evaluation of protective or damaging effects and the TCM action mechanism against $Yang_{syn}$ or Yin_{syn}. With a good description of the changes in the metabolic characteristics of endogenous metabolites and the differential expression changes of a series of functional genes in organisms, metabolomics and transcriptomics have been successfully applied to screen various diseases and their metabolic or gene profile changes in drug intervention (Lu et al., 2020; Ren et al., 2016). This study constructed $Yang_{syn}$ and Yin_{syn} animal models to evaluate whether the liver damage induced by BGZ is related to its non-symptomatic use and the possible susceptible individual characteristics.

2. Experiment

2.1 Chemicals and reagents

Hydrocortisone succinate sodium was provided by Tianjin Biochemical Pharmaceutical Co., Ltd. (Tianjin, China). Thyroxine and reserpine were provided by Shanghai MACKLIN Technology Co., Ltd. (Shanghai, China). Alanine aminotransferase (ALT), aspartate aminotransferase (AST), and serum creatinine (SCr) tests were purchased from Jiancheng Biological Technology, Co., Ltd. (Nanjing, China). Cyclic adenosine monophosphate (cAMP), and cyclic guanosine monophosphate (cGMP) were purchased from Mlbio Biotechnology Co., Ltd. (Shanghai, China).

2.2 BGZ Preparation

BGZ was purchased from the Anhui Puren Herbal Pieces Co., Ltd. (Anhui, China) and authenticated by Professor Xiaohe Xiao of the institute of Hepatology, Fifth Medical Center, PLA General Hospital (Beijing, China). In addition, BGZ was crushed and filtered through 200 mesh sieves and then suspended in 0.5% sodium carboxymethyl cellulose (CMC-Na) for administration.

2.3 Animal maintenance and treatment

Male Sprague–Dawley rats (180–200 g) were obtained from the SPF Biotechnology Co. Ltd. (License No. SCXK20190010, Beijing, China), and housed in the Laboratory Animal Center of the Fifth Medical Center, Chinese PLA General Hospital (animal ethics committee approval No. YFYDW2020017). All rats were raised

under specific pathogen-free conditions under a 12 h light/dark cycle, with free access to adequate food and water. All animals were fed adaptively for 1 week before starting the experiments.

The rats were randomly divided into six separate groups (N = 8) as follows: Control group (CON), BGZ group (BGZ), kidney-yang deficiency syndrome group ($Yang_{syn}$), kidney-yang deficiency syndrome-treated with BGZ group ($Yang_{syn}$+BGZ), kidney-yin deficiency syndrome group (Yin_{syn}); kidney-yin deficiency syndrome-treated with BGZ group (Yin_{syn}+BGZ). Rats in the treatment groups were consecutively administered intragastrically with BGZ suspension every afternoon for 21 consecutive days, while the control group received the same volume of 0.50% CMC-Na solution for the same amount of time. The changes in body weight were recorded before the end of the experiment. From the 8th day of administration, the $Yang_{syn}$ and $Yang_{syn}$+BGZ group rats were given 25 mg/kg hydrocortisone subcutaneously once a day for 14 consecutive days to prepare the $Yang_{syn}$ model (Zhang et al., 2019). From the 15th day of administration, the Yin_{syn} and Yin_{syn}+BGZ group rats were given thyroxine (16 mg/ml) and reserpine (1 mg/ml) at the dosage of 0.5 ml/100 g via gastric perfusion once a day for 7 consecutive days to prepare the Yin_{syn} model (Wang, P. et al., 2010). The CON and the BGZ groups were given the same volume of 0.50% CMC-Na solution.

2.4 Blood collection, organ index, and tissue preparation

After the experiment, all animals were anesthetized with 2% pentobarbital sodium. Blood samples with and without anticoagulants were collected, and the liver and kidney were weighed immediately after sacrifice to calculate the organ index. Partial liver tissue was collected for histological examination and the remaining liver was quickly frozen with liquid nitrogen and stored at -80°C until needed.

2.5 Serum biochemistry and histopathological analysis

After centrifugation (3500 rpm, 10 min, 4°C), serum biochemistry (ALT, AST, SCr) and neurotransmitters (cAMP, cGMP) were determined according to the microplate assay kit instructions, the left hepatic lobe was fixed with 4% paraformaldehyde for 48 h, embedded in wax, and sectioned at approximately 5 μm for Hematoxylin and Eosin (HE) pathological staining analysis.

2.6 RNA sequence analysis and data processing

Total RNA was extracted from liver tissues using Trizol reagent (Invitrogen, USA) according to the manufacturer's protocol, and genomic DNA was removed using DNase I (TaKara). RNA quality was assessed with a Bioanalyzer 2100 (Agilent) and measured with a NanoDrop 2000 spectrophotometer. Only a high-quality RNA sample ($OD_{260/280}$ = 1.8 ~ 2.2, $OD_{260/230} \geq 2.0$, RNA integrity number (RIN) ≥ 6.5, 28S:18S ≥ 1.0, > 1 μg) was used to construct the sequencing library. RNA-seq transcriptome libraries were prepared using a TruSeqTMRNA sample preparation kit from Illumina (San Diego, CA) and sequenced with the Illumina HiSeq xten/NovaSeq 6000 sequencer under standard protocols. All samples had a Q30 (bases of Q ≥ 30 /all bases of sequencing) of > 91%. Sequence readers were trimmed and quality controlled using SeqPrep (https://github.com/jstjohn/SeqPrep) and Sickle (https://github.com/najoshi/sickle) with default parameters and aligned to the reference genome through the orientation mode using hierarchical indexing for spliced alignment of transcripts 2 (HISAT2) (Kim et al., 2015). Messenger RNA levels were quantified using RSEM (http://deweylab.biostat.wisc.edu/rsem/) (Li and Dewey, 2011). Differentially expressed genes

(DEGs) were identified as those with | log2 (fold change) | >1 and *Padjust < = 0.05* (DESeq2) (Love et al., 2014).

2.7 Reverse transcription-quantitative polymerase chain reaction (RT-qPCR)

Liver tissue RNA was extracted by the Tissue RNA Purification Kit Plus (RN002plus, ES Science, China) and reverse-transcribed into cDNA using the Fast All-in-One RT Kit (RT001, ES Science, China) according to the manufacturer's instructions. The qPCR of aldehyde dehydrogenase 1 family member B1 (Aldh1b1), galectin 5 (Lgals5), solute carrier family 25 member 25 (Slc25a25), Pim-3 proto-oncogene, serine/threonine kinase (Pim3), and out at first (Oaf) were quantified by the SYBR Green PCR master mix (RN002plus, ES Science, China) with the QuantStudio 6 Flex PCR System (Applied Biosystems, USA). The amplification parameters were set according to the standard protocol. Primer sequences used in this study are shown in Supplemental Table 1. Relative gene expression was calculated using the $2^{-\triangle\triangle Ct}$ method $2^{-\Delta\Delta Ct}$ (Ish-Shalom and Lichter, 2010).

2.8 Liver sample processing

The liver was homogenized with normal saline at 1:1 (1g:1mL) using a homogenizer. The 300 uL homogenized sample and 900 uL methanol were mixed and vortexed for 30 s. The supernatant was centrifuged at 12000 r/min for 10 min and concentrated to dry using a vacuum centrifugal concentrator. Then 100 uL methanol was added for redissolving and centrifuged at 13000 r/min for 10 min. Finally, a 4 uL supernatant was taken out for UPLC-QTOF/MS (Waters, Manchester, UK) detection.

2.9 UPLC-QTOF/MS analysis and data processing

Metabolic profiling analysis of the biofluids was performed using the Waters Xevo G2-XS QTOF/MS (Waters, Manchester, UK). An analytical Acquity UPLC HSS T3 C18 column (temperature 30°C) was injected with 4 μL aliquots of each sample. For positive electrospray ionization source (ESI+) analysis, samples were isolated using a 30 min linear gradient of solvent A (water spiked with 0.1% formic acid) and solvent B (acetonitrile spiked with 0.1% formic acid) as mobile phases. The flow rate was fixed at 0.30 mL/min. For each sample, 10 μL was drawn as a quality control sample to ensure that the system was stable and the analyses were repeatable. Every 20th sample was injected with the control sample and subsequently analyzed. Masslynx software (v4.1, Waters Corp.) and Progenesis QI (v. 2.4, Waters Technologies, UK) were used for identifying the original mass spectral data and normalizing the total ion intensity of each chromatogram to acquire a data matrix containing the m/z value, retention time (RT), and normalized peak area. SIMCA-P 14.1 software (Umetrics, Umea, Sweden) was used for principal component analysis (PCA) and orthogonal partial least-squares discriminant analysis (OPLS-DA). The PCA score chart was used to show the natural interrelation of observation results. Variable importance in the projection (VIP) ≥ 1 and with significant differences between groups (*P < 0.05*) were selected as potential metabolites. Online metabolic databases including the Human Metabolome Database (HMDB) (http://www.hmdb.ca/) and Kyoto Encyclopedia of Genes and Genomes (KEGG) (https://www.genome.jp/kegg/) were combined with exact masses and secondary ion mass spectrometry of the metabolites acquired through Progenesis QI to identify the differential metabolites.

2.10 Statistical analysis

Statistical analysis was performed with Prism 8.0 (GraphPad Software, San Diego, CA). All results are expressed as mean ± SD. A one-way analysis of variance (ANOVA) was used to statistically analyze the multiple-group analysis. The student's t-test was used to statistically analyze the receiver operating characteristic (ROC) curve analysis. The significance threshold was set at $P < 0.05$.

3 Results

3.1 Effects of BGZ treatment on weight, anal temperature, and organ indexes of liver and kidney in Yin $_{syn}$ and Yang$_{syn}$ rats

As shown in Fig. 1A, compared with the CON group, the body weight of the BGZ group, Yang$_{syn}$ group, Yang$_{syn}$+BGZ group, and Yin$_{syn}$ group had no obvious changes, while the Yin$_{syn}$+BGZ group decreased significantly compared with the Yin$_{syn}$ group ($P < 0.01$). The anal temperature of rats in the Yang$_{syn}$ group and Yin$_{syn}$ group were significantly decreased and increased, respectively, compared with the CON group (both $P < 0.01$), while the anal temperature in the Yang$_{syn}$+BGZ group and Yin$_{syn}$+BGZ group were all significantly increased compared with the corresponding model groups (both $P < 0.05$) (Fig. 1B). As shown in Fig. 1C, the organ indexes of the liver in the Yang$_{syn}$ group and Yin$_{syn}$ group were all markedly increased compared with the CON group ($P < 0.001$, $P < 0.001$), and the liver organ indexes in the Yin$_{syn}$+BGZ group was further increased compared with the Yin$_{syn}$ group ($P < 0.001$), while there was also no changed in the Yang$_{syn}$+BGZ group compared with the Yang$_{syn}$ group. As for the kidney, only the Yin$_{syn}$ group had a significant increase in organ indexes compared with the CON group ($P < 0.001$) (Fig. 1D).

3.2 Effect of BGZ treatment on the serum levels of ALT, AST, SCr, and liver histopathological changes in Yin $_{syn}$ and Yang$_{syn}$ rats

Serum ALT, AST, and SCr, which are well-recognized markers of various types of liver and kidney damage, were used for the analysis. Regarding liver function (Fig. 2A-B), there were no obvious changes in the levels of ALT and AST between the BGZ group and the CON group. In contrast, the levels of ALT and AST in the Yang$_{syn}$ group increased prominently, while BGZ significantly reversed the phenomena (all $P < 0.05$). Though the AST level in the Yin$_{syn}$ group was significantly increased ($P < 0.01$), there was no obvious change in the levels of AST between the Yin$_{syn}$+BGZ group and the Yin$_{syn}$ group, while the ALT level was significantly increased after administration of BGZ in the Yin$_{syn}$+BGZ group ($P < 0.001$), illustrating that there was a certain risk of liver injury in rats with Yin$_{syn}$ after administration of BGZ. As for kidney function (Fig. 2C), no significant SCr changes were found in almost all groups except for the Yin$_{syn}$ group ($P < 0.001$). Combined with the changes in the kidney organ index, it revealed that BGZ may have no obvious renal toxicity in rats with Yang$_{syn}$ or Yin$_{syn}$.

As shown in Fig. 2D, the liver sections of the CON group showed normal hepatocyte structures. The liver samples from BGZ-treated rats were almost indistinguishable from normal rats. The liver samples from the

$Yang_{syn}$ group exhibited hepatocyte focal necrosis, loss of central vein intima, and inflammatory cell infiltration in portal vein areas, while the above symptoms were alleviated in the $Yang_{syn}$+BGZ group. The liver samples from the Yin_{syn} group exhibited slight inflammatory infiltration in the portal area but no evident hepatocyte injury, while the hepatocyte focal necrosis and inflammatory cell infiltration were aggravated in the Yin_{syn}+BGZ group. Combined with the levels of ALT, AST, liver index, and liver pathological examination, it was suggested that BGZ has a preferable liver protection effect on rats with $Yang_{syn}$ and a certain risk of liver injury effect on rats with Yin_{syn}.

3.3 DEG alterations of BGZ treatment in Yin_{syn} and $Yang_{syn}$ rats

To reveal the mechanism of different therapeutic effects of BGZ on Yin_{syn} and $Yang_{syn}$ rats, liver gene expression profiles were obtained from the CON, BGZ, $Yang_{syn}$, $Yang_{syn}$+BGZ, Yin_{syn}, and Yin_{syn}+BGZ groups using RNA-Seq analysis. As shown in Fig. 3A, compared with the CON group, BGZ barely influenced the gene expression with only 4 DEGs increased and 5 DEGs decreased, while 439 up-regulated DEGs and 652 down-regulated DEGs were found in the $Yang_{syn}$ group, and 508 up-regulated DEGs along with 847 down-regulated DEGs were found in the Yin_{syn} group. Compared to the $Yang_{syn}$ group, the number of up-regulated and down-regulated DEGs decreased to 59 and 43 by BGZ treatment, respectively, while for the Yin_{syn} group, the number of up-regulated and down-regulated DEGs decreased to 11 and 17 by BGZ treatment, respectively. To further display the above differences in DEGs more intuitively, heatmaps were constructed based on relative abundance (Fig. 3B and 3C).

3.4 Correlation analysis between DEGs and serum biochemistry

By analyzing the correlations between serum biochemistry (ALT and AST) and DEGs changed using BGZ in Yin_{syn} and $Yang_{syn}$ rats (Fig. 4), the results demonstrated that 36 DEGs, including 34 positive DEGs and 2 negative DEGs, were significantly correlated with ALT, and 12 DEGs, including 9 positive DEGs and 3 negative DEGs, were significantly correlated with AST. Among them, hyperpolarization-activated cyclic nucleotide-gated potassium channel 3 (Hcn3), aldehyde dehydrogenase 1 family member B1 (Aldh1b1), galectin 5 (Lgals5), solute carrier family 25 member 25 (Slc25a25), Pim-3 proto-oncogene, serine/threonine kinase (Pim3), and out at first (Oaf) were all significantly positively correlated with ALT and AST, and LOC100364769 was significantly negatively correlated with ALT and AST. The detailed relationship between DEGs and serum biochemistry (ALT and AST) was shown in Supplemental Table 2.

3.5 ROC curve analysis of DEGs

To further explore the diagnostic efficacy of DEGs, a ROC curve analysis was performed using GraphPad Prism software (version 8.01). The results revealed that 22 DEGs could be better discriminated between the $Yang_{syn}$+BGZ group and $Yang_{syn}$ group, and 10 DEGs had better discrimination between the Yin_{syn}+BGZ

group and Yin_{syn} group (all the areas under the curve (AUC) of the ROC curves ≥ 0.9 and $P < 0.05$) (Supplemental Fig. 1). Venn analysis showed the ROC results of DEGs and their correlation with the levels of ALT and AST between the $Yang_{syn}$+BGZ group and $Yang_{syn}$ group (Fig. 5A), revealing that Aldh1b1, Slc25a25, Pim3, and Oaf can be used as potential biomarkers for the treatment of $Yang_{syn}$ (Fig. 5B-E). Venn analysis also showed the ROC results of DEGs and their correlation with ALT and AST between the Yin_{syn}+BGZ group and Yin_{syn} group (Fig. 5J), revealing that Lgals5 may be used as a potential biomarker for the treatment of Yin_{syn} (Fig. 5K). As shown in Fig. 5F-I and 5L, the expression of Slec25a25, Pim3, and Oaf in rats with $Yang_{syn}$ and Yin_{syn} were all significantly increased compared with the CON group (all $P < 0.05$), while the level of Aldh1b1 in the $Yang_{syn}$ and the level of Lgals5 in the Yin_{syn} were all significantly decreased compared with the normal group (both $P < 0.05$). After BGZ intervention, the levels of Aldh1b1, Lgals5, Slec25a25, Pim3, and Oaf were all significantly decreased in the $Yang_{syn}$+BGZ group (all $P < 0.05$), while only Lgals5 was significantly increased in rats with Yin_{syn}+BGZ compared the Yin_{syn} group ($P < 0.05$).

3.6 GO and KEGG functional enrichment analysis of DEGs

Gene Ontology (GO) functional enrichment analysis (Fig. 6A) found that 95 GOs were significantly changed in the $Yang_{syn}$+BGZ group compared with the $Yang_{syn}$ group, such as GO:0009991 (response to extracellular stimulus), GO:0032922 (circadian regulation of gene expression), GO:0031667 (response to nutrient levels), and GO:0009892 (negative regulation of metabolic process), while 6 GOs including GO:0019825 (oxygen binding), GO:0020037 (heme-binding), GO:0046906 (tetrapyrrole binding), GO:0005833 (hemoglobin complex), GO:0005344 (oxygen carrier activity), and GO:0042743 (hydrogen peroxide metabolic process) were significantly changed in the Yin_{syn}+BGZ group compared with the Yin_{syn} group. Kyoto Encyclopedia of Genes and Genomes (KEGG) functional enrichment analysis (Fig. 6B) found that 4 KEGG orthologs (Kos) including ko00360 (phenylalanine metabolism), ko00350 (tyrosine metabolism), ko00380 (tryptophan metabolism), and ko00130 (ubiquinone and another terpenoid-quinone biosynthesis) were significantly changed in the $Yang_{syn}$+BGZ group compared with the $Yang_{syn}$ group, while 2 Kos including ko00260 (glycine, serine, and threonine metabolism) and ko00591 (linoleic acid metabolism) were significantly changed in the Yin_{syn}+BGZ group compared with the Yin_{syn} group.

3.7 Metabolomic analysis of BGZ treatment in Yin_{syn} and $Yang_{syn}$ rats

As shown in Fig. 7A and 7B, the QC samples gathered closely in both PCA score plots, indicating the stability of the UPLC-QTOF/MS system throughout the analysis. The CON, $Yang_{syn}$, and Yin_{syn} groups can be well distinguished, suggesting that the metabolic information between the $Yang_{syn}$ and Yin_{syn} groups has been changed. OPLS-DA analysis found that the comparison between the $Yang_{syn}$ group and the $Yang_{syn}$+BGZ groups (Fig. 7C and 7D) could both be significantly separated under ESI + and ESI- modes, and the comparison between the Yin_{syn} group and Yin_{syn}+BGZ group (Fig. 7E and 7F) could also both be significantly separated under ESI + and ESI- modes, and the permutation tests for OPLS-DA analysis revealed the models were not overfitted (Supplemental Fig. 2), indicating that significant metabolic

disturbance occurred in the $Yang_{syn}$ group and Yin_{syn} group after BGZ treatment. A total of 40 metabolites were identified based on *m/z* and corresponding secondary fragment ion characteristic maps (Table 1, Supplemental Fig. 3). Among the metabolites, 27 metabolites were markedly changed in the $Yang_{syn}$+GBZ group compared with the $Yang_{syn}$ group, and 31 metabolites were significantly changed in the Yin_{syn}+GBZ group compared with the Yin_{syn} group. The heatmap for the above differential metabolites is presented in Fig. 7G.

Table 1
Identified differential metabolites.

ESI	m/z	RT (min)	KEGG	Metabolite	($Yang_{syn}$+BGZ) vs ($Yang_{syn}$)	(Yin_{syn}+BGZ) vs (Yin_{syn})
-	145.0132	0.9378	C00026	α-Ketoglutarate	↑*	↓
-	455.0965	2.9226	C00061	Riboflavin-5-phosphate	↑*	↓*
-	104.0348	0.8028	C00065	L-Serine	↑	↓*
+	113.0352	0.9136	C00106	Uracil	↓*	↑*
+	778.5407	13.2262	C00157	Phosphatidylcholine	↑	↓
-	582.5100	13.2602	C00195	N-Acylsphingosine	↑**	↓*
-	148.0378	1.3859	C00250	Pyridoxal	↑*	↓*
-	243.0615	1.3509	C00299	Uridine	↓	↑*
-	102.0556	0.8313	C00334	gamma-Aminobutyric acid	↑*	↓*
-	766.6037	9.3765	C00350	Phosphatidylethanolamine	↓**	↑*
-	240.0224	1.5073	C00352	Glucosamine 6-phosphate	↑*	↓**
-	151.0569	0.9235	C00379	D-Xylitol	↑	↓*
-	671.4653	13.3460	C00416	Phosphatidate	↓***	↑*
+	173.0922	0.8994	C00430	5-Aminolevulinate	↓**	↑
+	160.0756	1.9497	C00483	Tyramine	↓*	↑*
-	583.2469	8.6720	C00486	Bilirubin	↑	↓*
+	583.2554	8.0917	C00500	Biliverdin	↑**	↓*
+	90.0555	0.8565	C00546	Methylglyoxal	↑	↓*
-	397.2291	11.6884	C00584	Prostaglandin E2	↓**	↑*
-	229.0667	1.6209	C00588	Phosphorylcholine	↑*	↓*
+	426.3162	15.2409	C00695	Cholic acid	↑	↓**
+	252.0724	2.1330	C00818	Glucaric acid	↑	↓*
+	465.3556	11.5639	C01724	Lanosterin	↑	↓*
+	799.6627	15.2528	C01829	Thyroxine	↑**	↓
+	196.0943	4.0050	C03264	D-Leucate	↑**	↓
-	187.1076	1.3080	C02727	N6-Acetyl-L-lysine	↑*	↓*

*$P < 0.05$, **$P < 0.01$, ***$P < 0.001$.

ESI	m/z	RT (min)	KEGG	Metabolite	($Yang_{syn}$+BGZ) vs ($Yang_{syn}$)	(Yin_{syn}+BGZ) vs (Yin_{syn})
+	560.3333	8.4013	C03033	beta-D-Glucuronoside	↑*	↓
-	205.0645	1.7274	C03227	3-Hydroxy-L-kynurenine	↓*	↑*
+	522.3564	9.5634	C04230	1-Acyl-sn-glycero-3-phosphocholine	↑**	↓
-	401.0785	6.4160	C04352	(R)-4'-Phosphopantothenoyl-L-cysteine	↑**	↓***
+	381.0794	0.9636	C04778	N1-(5-Phospho-a-D-ribosyl)-5,6-dimethylbenzimidazole	↓*	↑**
-	347.1835	8.9063	C05302	2-Methoxyestradiol	↑	↓**
-	526.0585	1.3859	C05381	3-Carboxy-1-hydroxypropylthiamine diphosphate	↓	↑*
+	389.2142	4.7813	C05476	Tetrahydrocorticosterone	↑**	↓
-	183.0346	0.8099	C05580	3,4-Dihydroxymandelate	↓	↑*
-	297.0703	0.9593	C05648	5-Hydroxy-N-formylkynurenine	↑	↓*
-	577.3444	13.7089	C05789	L-Urobilinogen	↓*	↑
-	365.2324	6.4089	C14777	12(S)-HETE	↓*	↑*
+	353.2472	6.4221	C16513	Docosapentaenoic acid (22n-3)	↑*	↓*
+	136.0396	1.6256	C22040	Methylcysteine	↑*	↓**

**P < 0.05*, ***P < 0.01*, ****P < 0.001*.

3.8 Correlation analysis between metabolites and serum biochemistry

By analyzing the correlations between serum biochemistry (ALT and AST) and differential metabolites (Fig. 8), 20 metabolites, including 3 positive and 17 negative correlations, were significantly correlated with ALT, and 12 metabolites, including 3 positive and 9 negative correlations, were significantly correlated with AST. The correlation coefficient r and *P-value* are shown in Supplemental Table 3. Among them, Phosphatidate, Uracil, Prostaglandin E2, and N1-(5-Phospho-a-D-ribosyl)-5,6-dimethylbenzimidazole were all significantly positively correlated with ALT and AST, and Phosphatidylcholine, Lanosterin, N-Acylsphingosine, D-Leucate, Gamma-aminobutyric acid, Biliverdin, beta-D-Glucuronoside, and Docosapentaenoic acid (22n-3) were all significantly negatively correlated with ALT and AST.

3.9 ROC curve analysis of metabolites

As shown in Supplemental Fig. 4, 9 metabolites had better discrimination between the $Yang_{syn}$+BGZ group and $Yang_{syn}$ group, and 5 metabolites had better discrimination between the Yin_{syn}+BGZ group and Yin_{syn} group (all the areas under the curve (AUC) of the ROC curves ≥ 0.9 and $P < 0.05$). Venn analysis showed the ROC results of metabolites and their correlation with the levels of ALT and AST among the comparison of the $Yang_{syn}$+BGZ group and $Yang_{syn}$ group (Fig. 9A) and the comparison of the Yin_{syn}+BGZ group and the Yin_{syn} group (Fig. 9F). Among them, Phosphatidate, Phosphatidylcholine, D-Leucate, and Biliverdin may be used as potential hepatoprotective biomarkers for the treatment of $Yang_{syn}$ (Fig. 9B-E), while N1-(5-Phospho-a-D-ribosyl)-5,6-dimethylbenzimidazole may be used as a potential hepatotoxicity biomarker for the treatment of Yin_{syn} (Fig. 9G).

3.10 Comparison of overall metabolic profiles

To further understand the metabolic disorder of susceptible syndromes, the KEGG identification code of differential metabolites was used for pathway analysis via MetaboAnalyst 5.0 (https://www.metaboanalyst.ca/). The schematic diagram of the disturbed metabolic pathways changed by the treatment of BGZ for $Yang_{syn}$ and Yin_{syn} rats is presented in Fig. 10A and 10B. The redder the bubble color, the smaller the *P* value of the metabolic pathway. The details for the value of *P* are shown in Supplemental Tables 4 and 5. The results indicated that there are significant differences in glycerophospholipid metabolism, arachidonic acid metabolism, pantothenate, and CoA biosynthesis pathways in the $Yang_{syn}$+BGZ group compared with the $Yang_{syn}$ group, while pantothenate and the CoA biosynthesis pathway were significantly changed in the Yin_{syn}+BGZ group compared with the Yin_{syn} group. To compare the differences in metabolic profiles for BGZ treatment on Yin_{syn} and $Yang_{syn}$ rats, a network map was constructed based on the identified metabolites and enriched metabolic pathways. As shown in Fig. 10C, metabolic pathways and metabolites interacted with each other to form a complex network.

3.11 Integration analysis of metabolite and DEGs enrichment pathway.

The expression changes of metabolites and DEGs in vivo can affect each other and cause a series of changes in body function. It is worth noting that, the pathways of BGZ regulating in rats with Yin_{syn} and $Yang_{syn}$ are almost all involved in energy metabolism, amino acid metabolism, lipid metabolism, and metabolism of cofactors and vitamins (Fig. 11A), and the above pathways were also cross-regulated by the “second messenger” of cAMP and cGMP (Cheng et al., 2019; Godfrey et al., 1987; Shen et al., 2011) (Fig. 11B). As shown in Fig. 11C-E, the study further found the protein expression cAMP was significantly decreased in the $Yang_{syn}$ group ($P < 0.01$) and increased in the Yin_{syn} group ($P < 0.05$) while compared with the CON group. Meanwhile, the protein levels of cGMP were significantly increased in both model groups (both $P < 0.05$), accompanied by a significantly decreased ratio of cAMP/cGMP in the $Yang_{syn}$ group ($P < 0.001$). The changes in levels of cAMP, cGMP, and cAMP/cGMP ratio are consistent with the changes in Yin_{syn} and $Yang_{syn}$ models and are often used as indicators to evaluate the above syndrome models (Averaimo and Nicol, 2014). After BGZ intervention, there was no significant change in cGMP in the two

model groups, while the levels of cAMP and cAMP/cGMP in the $Yang_{syn}$+BGZ group and Yin_{syn}+BGZ group were all significantly increased or decreased compared with corresponding models, respectively (all $P < 0.05$).

4 Discussion

Individual variability in liver injury following drug ingestion is a major challenge for DILI research and clinical prevention (Andrade et al., 2019). In the study, it was found that Yin_{syn} and $Yang_{syn}$ are two different predisposed individual states of hepatotoxicity or hepatoprotection caused by BGZ. From the perspective of the gene expression profile, BGZ mostly does not affect normal rats, but it has a mild or greater impact on the change numbers of DEGs in Yin_{syn} (28 DEGs) and $Yang_{syn}$ (102 DEGs) rats, respectively. From the perspective of endogenous metabolites, Yin_{syn} and $Yang_{syn}$ rats can be well distinguished on the PCA scatter plot, and the OPLS-DA plot can further better distinguish Yin_{syn}, $Yang_{syn}$, and their corresponding BGZ-treated groups, suggesting that BGZ exerts different metabolic perturbation patterns for different models.

Among the DEGs with ROC ≥ 0.9 and significant correlation with ALT and AST, Slc25a25 may function as an ATP-Mg/Pi carrier to mediate the transport of Mg-ATP in exchange for phosphate. It is also likely responsible for the net uptake or efflux of adenine nucleotides into or from the mitochondria and is highly expressive in acute liver failure or induced by exogenous thyroxine (Fujimoto et al., 2018; Lee et al., 2022). This study confirmed the high expression of Slc25a25 in the liver of Yin_{syn} and $Yang_{syn}$ rats, which is consistent with the phenomenon of abnormal liver function (Lee et al., 2022). However, only the expression of Slc25a25 in $Yang_{syn}$ rats was inhibited by BGZ, indicating that Slc25a25 may be a hepatoprotective gene for BGZ in $Yang_{syn}$ rats, and the way to aggravate liver injury in rats with Yin_{syn} may not be through regulating Slc25a25.

Pim3 is a liver growth-stimulating factor with serine/threonine kinase activity and is involved in gp130-mediated induction of cell proliferation and protection of apoptosis downstream of signal transducer and activator of transcription 3 (STAT3) (Liu et al., 2018; Wang et al., 2019). Pim3 is barely expressed in normal tissues but highly expressed in the prostate, large intestine, liver, and other cancer tissues (Brault et al., 2010). Therefore, its expression l evel is mainly used to evaluate tumor expression and metastasis (Qu et al., 2016; Zhou et al., 2016). Epidemiological studies have found and confirmed the correlations between tumors and the constitution of Yin_{syn} and $Yang_{syn}$ (Chen and Wang, 2012; Ji et al., 2016). This study also found that Pim3 was abnormally highly expressed in the liver of Yin_{syn} and $Yang_{syn}$ rats, suggesting that Yin_{syn} and $Yang_{syn}$ may be susceptible to constitutions that induce tumors. Surprisingly, BGZ only decreased the expression of Pim3 in $Yang_{syn}$ rats with almost no change in Yin_{syn} rats. The above results indicated that Pim3 may be a marker gene for BGZ to exert a hepatoprotective effect on $Yang_{syn}$ rats. In addition, BGZ may also have a potential therapeutic effect on tumor patients with $Yang_{syn}$, and the anti-tumor effect of BGZ has been confirmed (Wu et al., 2013; Yu et al., 2019).

Among the metabolites with ROC > 0.90 and significant correlation with ALT and AST, glycerophospholipids (including phosphatidylcholine, phosphatidylethanolamine, and phosphatidylserine) are the most abundant phospholipids in the body. In addition to constituting biofilm, they are also one of the components of bile and membrane surface-active substances and participate in protein recognition and signal transduction through the cell membrane (Hishikawa et al., 2014). Hepatocytes can express various glycerophospholipids activities, making the liver an important organ for glycerophospholipid metabolism. Dysregulation of glycerophospholipids is related to the development and progression of liver diseases including hepatitis, liver cancer, fatty liver, and liver fibrosis (van der Veen et al., 2017). For example, the abnormal increase or decrease of the ratio of phosphatidylcholine (PC) to phosphatidylethanolamine (PE) will affect energy metabolism and are closely related to disease progression (Li et al., 2006). The changes in hepatic phospholipid composition are also associated with fatty liver disease and impaired postoperative liver regeneration (Clemens et al., 2021; Ling et al., 2012; Sasabe et al., 2014). In the glycerophospholipid metabolic pathway, phosphatidate can activate hepatic interleukin 6 (IL-6) signaling through inter-organ crosstalk and alleviating acetaminophen-induced liver injury in mice (Clemens et al., 2021). Phosphatidate also acts as an ionophore in the brain between depolarization and the release of neurotransmitters such as gamma-Aminobutyric Acid (GABA) (Harris et al., 1981). The increase in the level of GABA can enhance the body's immunity under stress conditions (Abdou et al., 2006) and has a good protective effect on acute liver injury or liver failure induced by ethanol, fluoride, and d-galactosamine (Hata et al., 2019; Wang et al., 2018; Yang et al., 2017). In this study, under the intervention of BGZ, the expression of PE and GABA in the liver of rats with Yin_{syn} and $Yang_{syn}$ both showed opposite trends, suggesting that regulating glycerophospholipid metabolism may be another way in which BGZ exerts liver protection and liver injury in $Yang_{syn}$ and Yin_{syn} rats, respectively.

The metabolites of lipid metabolism participate in the biosynthesis of glycerophospholipid metabolism together with serine, providing raw materials for its metabolism (Cook et al., 1991). The metabolism of arachidonic acid, sphingolipid, glycine, serine, threonine, porphyrin, and chlorophyll can also interact directly or indirectly through serine. In the arachidonic acid metabolic pathway, 12(S)-HETE, as an important inflammatory marker, can affect the inflammatory process by stimulating the release of cytokines such as tumor necrosis factor alpha-like (TNF-α) and IL-6. Blocking the production of 12(S)-HETE can inhibit ischemia-reperfusion-induced liver dysfunction, inflammation, and cell death (Zhang et al., 2018). As a regulatory enzyme of arachidonic acid metabolism, arachidonate 15-lipoxygenase (Alox15) can catalyze it to 12(S)-HPETE, which is further reduced by glutathione peroxidase into 12(S)-HETE (Spector et al., 1988). Prostaglandin E2 (PGE2), another metabolite of arachidonic acid, has also been shown to induce acute and chronic inflammation and various autoimmune diseases through Th1 differentiation, Th17 cell proliferation, and activation of mast cells (Tsuge et al., 2019). In this study, the expressions of 12(S)-HETE, PGE2, and Alox15 were significantly increased in the Yin_{syn} group under the intervention of BGZ, while the expressions of 12(S)-HETE, PGE2, and Alox15 were significantly decreased or did not change significantly in the $Yang_{syn}$ group, suggesting that the regulation of arachidonic acid metabolism may be another way in which BGZ regulates the effects of liver protection or liver damage in rats with $Yang_{syn}$ and Yin_{syn}, respectively.

In the metabolic pathway of porphyrin and chlorophyll, 5-aminolevulinate, the direct metabolite of glycine, can be used as a precursor of heme and participate in the regulation of the production of heme and its metabolite biliverdin (Sansaloni-Pastor et al., 2022). Biliverdin has a good anti-inflammatory effect, can inhibit the expression of toll-like receptor 4 and nitric oxide, and reduces the inflammatory induction of lipopolysaccharide on macrophages (Wegiel et al., 2011). It is used in the protection against various diseases (vascular injury, organ transplantation, etc.). As such, biliverdin can better reduce the ischemia-reperfusion injury in pig liver and have a liver protective effect (Andria et al., 2013). Biliverdin reductase B (Blvrb) is a non-redundant nicotinamide adenine dinucleotide (phosphate)-dependent biliverdin reductase that regulates the cellular redox state by converting biliverdin to bilirubin. Tts redox function also reduces intracellular reactive oxygen species accumulation (Wu et al., 2016) and maintains essential cytoprotective functions in recovery from hematopoietic stress (Nesbitt et al., 2021). Bilirubin is the main pigment in human bile and the main metabolite of iron porphyrin compounds in the body with certain damage to the brain and nerves (Watchko and Tiribelli, 2013). The increase in its level can also lead to impaired liver function, so it is also used as a test for one of the common indicators of jaundice (Fawaz et al., 2017). In the study, BGZ significantly increased the expressions of biliverdin in $Yang_{syn}$ rats accompanied by the inhibition expressions of bilirubin in Yin_{syn} rats, suggesting that the regulation of porphyrin metabolism, especially Blvrb, may be a mechanism by which BGZ exerts hepatoprotective or liver damage effects on $Yang_{syn}$ and Yin_{syn} rats, respectively. However, this is not related to bilirubin.

Tryptophan is involved in immune regulation, neural function, and intestinal homeostasis through the kynurenine pathway for metabolism (Cervenka et al., 2017). For example, kynurenine is an endothelium-derived relaxation factor in the inflammatory process (Wang, Y. et al., 2010) and is metabolized to neurotoxic 3-Hydroxy-L-kynurenine under the action of kynureninase (Kynu), which is involved in the inflammatory process in psoriasis and other inflammatory diseases (Harden et al., 2016). Therefore, the imbalance of tryptophan metabolism in diseases ranging from cancer to neurodegenerative diseases has become a research hotspot for the therapeutic targeting of the kynurenine pathway (Platten et al., 2019). In this study, compared with the $Yang_{syn}$ group and the Yin_{syn} group, the levels of 3-Hydroxy-L-kynurenine were significantly decreased and increased under the intervention of BGZ, respectively, suggesting the kynurenine metabolism pathway in regulating tryptophan metabolism may be another mechanism by which BGZ exerts hepatoprotective or liver damage effects on $Yang_{syn}$ and Yin_{syn} rats.

The above-discussed pathways changed by BGZ in Yin_{syn} and (or) $Yang_{syn}$, were almost all related to energy metabolism, amino acid metabolism, and lipid metabolism, and the disorder of the above pathways has also been reported in Yin_{syn} and $Yang_{syn}$ (Chen et al., 2019; Jiang et al., 2015). The effects of BGZ on the metabolism of the above pathways have also been reported by Xu et al. (Xu et al., 2017). cAMP and cGMP, the potential biomarkers for Yin/Yang disharmony in TCM (Wang et al., 2021), can cross-activate protein kinases related to tissue biosynthesis and metabolism (including carbohydrate, lipid, amino acid, cofactors, and vitamins) as cyclic nucleotide effectors (Coelho Horta et al., 2005; Francis and Corbin, 1999; Jiang et al., 1992). Considering that BGZ can enhance the expression of cAMP-responsive element modulator-τ (CREMτ) (Wei et al., 2011), and the ability of BGZ to down-regulate and up-regulate the expression of cAMP and the ratio of cAMP/cGMP in rats with Yin_{syn} and $Yang_{syn}$, respectively. It is suggested that the cAMP signaling

pathway may be one of the mechanisms by which BGZ regulates energy metabolism to affect rats with Yin_{syn} or $Yang_{syn}$. As for the different intervention effects of BGZ on the different syndromes, the interaction of endogenous metabolites and genes may be the main reason, which is worthy of further study in the future.

In conclusion, this study found that BGZ has a double-edged sword-like effect that not only exerts a good hepatoprotective effect on $Yang_{syn}$ rats but also has a potential risk of inducing liver injury in Yin_{syn} rats. The mechanism is mainly reflected in BGZ having different regulatory effects on amino acid metabolism, energy metabolism, lipid metabolism, and metabolism of cofactors and vitamins in the above two different syndromes. In response to the seemingly contradictory results that BGZ has both liver-damaging and liver-protective effects in previous reports (Wang et al., 2020; Zhang et al., 2016), this study found that BGZ may have both liver-damaging and liver-protecting effects on predisposed individuals from the perspective of TCM syndrome theory. The study screened out the endogenous markers that can characterize the corresponding predisposed individuals, which will provide a certain reference for the safe and rational application of TCM.

Abbreviations

Psoralea corylifolia Linn.
BGZ
$Yang_{syn}$
kidney-yang deficiency syndrome
Yin_{syn}
kidney-yin deficiency syndrome
TCM
Traditional Chinese Medicine
HE
Hematoxylin and eosin
HMDB
Human Metabolome Database
KEGG
Kyoto Encyclopedia of Genes and Genomes
PCA
Principal components analysis
OPLS-DA
Orthogonal partial least-squares discriminate
VIP
variable importance in the projection
UPLC
Ultra-performance liquid chromatography
LC-MS

Liquid chromatography-tandem mass spectrometry
DILI
Drug-induced liver injury
GC
glucocorticoid
ALT
Alanine aminotransferase
AST
Aspartate aminotransferase
Scr
Serum creatinine
cAMP
cyclic adenosine monophosphate
cGMP
cyclic guanosine monophosphate
DEGs
Differentially expressed genes
ESI+
Positive electrospray ionization source
ROC
Receiver operating characteristic
GO
Gene Ontology
Kos
KEGG orthology
AUC
Areas under the curve
PGE2
Prostaglandin E2

Declarations

Ethics approval and consent to participate

Experimental animal protocols were approved by the Animal Ethics Committee of the First Affiliated Hospital of Henan University of Traditional Chinese Medicine and the procedures were conformed to the Guide for the Care and Use of Laboratory Animals.

Consent for publication

The authors declare that they have no competing interests.

Competing interests

The authors declare no competing financial interest.

Funding

This work was supported by the National Natural Science Foundation of China (No. 82173993, No. U1904129, No. 82204638, No. 82230118), the Key Project of Henan Province for Scientific Research of Traditional Chinese Medicine, China (No. 2019ZYBJ08), and the Key Scientific Research Projects of Colleges and Universities in Henan Province, China (No. 19A360007).

Authors' contributions

Jin-Fa Tang, Xiao-He Xiao, and Yan-Ling Zhao conceived and designed the experiments; Ming-Liang Zhang performed the experiments, analyzed the data, and wrote the manuscript; De-Xin Kong, Yuan Gao was responsible for helping the collection of experimental samples; Yu-Long Chen, Hui Zhang, Xiao-Yan Wang help to detect the metabonomic changes of liver samples, Xu Zhao and Ming Niu helped with data analysis, Zhao-Fang Bai, Wei-Xia Li, and Yu-Ming Guo reviewed the paper. All authors have reviewed the manuscript and approved the final version of the manuscript. All authors have read, revised, and approved the final manuscript.

Acknowledgments

We thank James thompson, PhD, from BEIJING LANGYI TRANSLATION CO., LTD., China, for mother tongue polishing the English text of this manuscript.

Availability of data and material

The research data generated from this study are included in the article and additional files.

References

1. Abdou AM, Higashiguchi S, Horie K, Kim M, Hatta H, Yokogoshi H. 2006. Relaxation and immunity enhancement effects of gamma-aminobutyric acid (GABA) administration in humans. BioFactors 26(3), 201–208.
2. Andrade RJ, Chalasani N, Björnsson ES, Suzuki A, Kullak-Ublick GA, Watkins PB, Devarbhavi H, Merz M, Lucena MI, Kaplowitz N, Aithal GP. Drug-induced liver injury. Nat Rev Dis Primers. 2019;5(1):58.
3. Andria B, Bracco A, Attanasio C, Castaldo S, Cerrito MG, Cozzolino S, Di Napoli D, Giovannoni R, Mancini A, Musumeci A, Mezza E, Nasti M, Scuderi V, Staibano S, Lavitrano M, Otterbein LE, Calise F. Biliverdin protects against liver ischemia reperfusion injury in swine. PLoS ONE. 2013;8(7):e69972.
4. Averaimo S, Nicol X. Intermingled cAMP, cGMP and calcium spatiotemporal dynamics in developing neuronal circuits. Front Cell Neurosci. 2014;8:376.
5. Brault L, Gasser C, Bracher F, Huber K, Knapp S, Schwaller J. PIM serine/threonine kinases in the pathogenesis and therapy of hematologic malignancies and solid cancers. Haematologica. 2010;95(6):1004–15.

6. Cervenka I, Agudelo LZ, Ruas JL. Kynurenines: Tryptophan's metabolites in exercise, inflammation, and mental health. Science. 2017;357(6349):eaaf9794.
7. Chen M, Borlak J, Tong W. High lipophilicity and high daily dose of oral medications are associated with significant risk for drug-induced liver injury. Hepatology. 2013;58(1):388–96.
8. Chen M, Borlak J, Tong W. A Model to predict severity of drug-induced liver injury in humans. Hepatology. 2016;64(3):931–40.
9. Chen M, Suzuki A, Borlak J, Andrade RJ, Lucena MI. Drug-induced liver injury: Interactions between drug properties and host factors. J Hepatol. 2015;63(2):503–14.
10. Chen R, Wang J, Zhan R, Zhang L, Wang X. Integrated Systems Pharmacology, Urinary Metabonomics, and Quantitative Real-Time PCR Analysis to Uncover Targets and Metabolic Pathways of the You-Gui Pill in Treating Kidney-Yang Deficiency Syndrome. Int J Mol Sci. 2019;20(15):3655.
11. Chen Z, Wang P. 2012. Clinical Distribution and Molecular Basis of Traditional Chinese Medicine ZHENG in Cancer. Evid Based Complement Alternat Med 2012, 783923.
12. Cheng ZX, Guo C, Chen ZG, Yang TC, Zhang JY, Wang J, Zhu JX, Li D, Zhang TT, Li H, Peng B, Peng XX. Glycine, serine and threonine metabolism confounds efficacy of complement-mediated killing. Nat Commun. 2019;10(1):3325.
13. Chinese Pharmacopoeia, Commission. 2020. Pharmacopoeia of the People's Republic of China. Beijing: Chinese Medical Science and Technology Press, 2020;1:195.
14. Clemens MM, Kennon-McGill S, Vazquez JH, Stephens OW, Peterson EA, Johann DJ, Allard FD, Yee EU, McCullough SS, James LP, Finck BN, McGill MR. Exogenous phosphatidic acid reduces acetaminophen-induced liver injury in mice by activating hepatic interleukin-6 signaling through inter-organ crosstalk. Acta Pharm Sinica B. 2021;11(12):3836–46.
15. Coelho Horta B, Perilo S, Caldeira Costa C, Nogueira-Machado D, Martins Chaves JA, M. Aging: functional metabolic balance among cAMP, cGMP and reactive oxygen intermediate generation by human granulocytes. Gerontology. 2005;51(6):363–8.
16. Cook HW, Thomas SE, Xu Z. Essential fatty acids and serine as plasmalogen precursors in relation to competing metabolic pathways. Biochem Cell Biol. 1991;69(7):475–84.
17. Deng PY, Cai HD, Cheng JH, Liu SA, Dao WB. 1996. Liver Damage Caused by Zhuanggu Joint Pill: A Report of 30 Cases. Chin J of New Drugs (03), 212–214.
18. Dermatology Branch of China Association of Chinese Medicine. Expert Consensus on Chinese Medicine Treatment of Vitiligo. Chin J Dermato Veneral Integ Trad W Med. 2017;16(02):191–2.
19. Dermatology Branch of China Association of Chinese Medicine. Expert consensus on traditional Chinese medicine treatment of psoriasis in Dermatology Branch. Chin J Dermato Venemol Integ Trad W Med. 2018;17(03):273–7.
20. Fawaz R, Baumann U, Ekong U, Fischler B, Hadzic N, Mack CL, McLin VA, Molleston JP, Neimark E, Ng VL, Karpen SJ. Guideline for the Evaluation of Cholestatic Jaundice in Infants: Joint Recommendations of the North American Society for Pediatric Gastroenterology, Hepatology, and Nutrition and the European Society for Pediatric Gastroenterology, Hepatology, and Nutrition. J Pediatr Gastroenterol Nutr. 2017;64(1):154–68.

21. Francis SH, Corbin JD. Cyclic nucleotide-dependent protein kinases: intracellular receptors for cAMP and cGMP action. Crit Rev Clin Lab Sci. 1999;36(4):275–328.
22. Fujimoto N, Kitamura S, Uramaru N, Miyagawa S, Iguchi T. Identification of hepatic thyroid hormone-responsive genes in neonatal rats: Potential targets for thyroid hormone-disrupting chemicals. Toxicol Lett. 2018;286:48–53.
23. Ge FL, Niu M, Han ZX, Cao JL, Wang JB, Bai ZF, Song HB, Guo YM, Xiao XH. Landscape of Hepatobiliary Adverse Drug Reactions Related to Preparations Containing Psoraleae Fructus and Its Application in Pharmacovigilance. Chin J Integr Med. 2021;27(11):832–7.
24. Ge JR, Wang HM, Zheng HX, Luo YW, Wang JB, Zhao YF, Wan XM, Lu M, He CJ, Dong Z, Zhou HJ, Li G, Sun SB, Lin XS. Traditional Chinese Medicine Expert Consensus on the prevention and treatment of primary osteoporosis. Chin J Osteoporos. 2020;26(12):1717–25.
25. Godfrey RW, Manzi RM, Gennaro DE, Hoffstein ST. Phospholipid and arachidonic acid metabolism in zymosan-stimulated human monocytes: modulation by cAMP. J Cell Physiol. 1987;131(3):384–92.
26. Gupta AK, Anderson TF. Psoralen photochemotherapy. J Am Acad Dermatol. 1987;17(5 Pt 1):703–34.
27. Harden JL, Lewis SM, Lish SR, Suárez-Fariñas M, Gareau D, Lentini T, Johnson-Huang LM, Krueger JG, Lowes MA. The tryptophan metabolism enzyme L-kynureninase is a novel inflammatory factor in psoriasis and other inflammatory diseases. J Allergy Clin Immunol. 2016;137(6):1830–40.
28. Harris RA, Schmidt J, Hitzemann BA, Hitzemann RJ. Phosphatidate as a molecular link between depolarization and neurotransmitter release in the brain. Science. 1981;212(4500):1290–1.
29. Hata T, Rehman F, Hori T, Nguyen JH. GABA, γ-Aminobutyric Acid, Protects Against Severe Liver Injury. J Surg Res. 2019;236:172–83.
30. Hishikawa D, Hashidate T, Shimizu T, Shindou H. Diversity and function of membrane glycerophospholipids generated by the remodeling pathway in mammalian cells. J Lipid Res. 2014;55(5):799–807.
31. Hoofnagle JH, Björnsson ES. Drug-Induced Liver Injury - Types and Phenotypes. N Engl J Med. 2019;381(3):264–73.
32. Ish-Shalom S, Lichter A. Analysis of fungal gene expression by Real Time quantitative PCR. Methods Mol Biol. 2010;638:103–14.
33. Ji Q, Luo YQ, Wang WH, Liu X, Li Q, Su SB. Research advances in traditional Chinese medicine syndromes in cancer patients. J Integr Med. 2016;14(1):12–21.
34. Jiang H, Shabb JB, Corbin JD. Cross-activation: overriding cAMP/cGMP selectivities of protein kinases in tissues. Biochem Cell Biol. 1992;70(12):1283–9.
35. Jiang N, Liu HF, Li SD, Zhou WX, Zhang YX, Zhang Q, Yan XZ. An integrated metabonomic and proteomic study on Kidney-Yin Deficiency Syndrome patients with diabetes mellitus in China. Acta Pharmacol Sin. 2015;36(6):689–98.
36. Kim D, Langmead B, Salzberg SL. HISAT: a fast spliced aligner with low memory requirements. Nat Methods. 2015;12(4):357–60.

37. Lee YM, Choi DH, Cheon MW, Kim JG, Kim JS, Shin MG, Kim HR, Youn D. 2022. Changes in Mitochondria-Related Gene Expression upon Acupuncture at LR3 in the D-Galactosamine-Induced Liver Damage Rat Model. Evid Based Complement Alternat Med 2022, 3294273.
38. Li B, Dewey CN. RSEM: accurate transcript quantification from RNA-Seq data with or without a reference genome. BMC Bioinformatics. 2011;12:323.
39. Li CY, Niu M, Liu YL, Tang JF, Chen W, Qian G, Zhang MY, Shi YF, Lin JZ, Li XJ, Li RS, Xiao XH, Li GH, Wang JB. Screening for Susceptibility-Related Factors and Biomarkers of Xianling Gubao Capsule-Induced Liver Injury. Front Pharmacol. 2020;11:810.
40. Li Z, Agellon LB, Allen TM, Umeda M, Jewell L, Mason A, Vance DE. The ratio of phosphatidylcholine to phosphatidylethanolamine influences membrane integrity and steatohepatitis. Cell Metab. 2006;3(5):321–31.
41. Li ZJ, Abulizi A, Zhao GL, Wang T, Zhou F, Jiang ZZ, Aibai S, Zhang LY. Bakuchiol Contributes to the Hepatotoxicity of Psoralea corylifolia in Rats. Phytother Res. 2017;31(8):1265–72.
42. Ling J, Chaba T, Zhu LF, Jacobs RL, Vance DE. Hepatic ratio of phosphatidylcholine to phosphatidylethanolamine predicts survival after partial hepatectomy in mice. Hepatology. 2012;55(4):1094–102.
43. Liu J, Qu X, Shao L, Hu Y, Yu X, Lan P, Guo Q, Han Q, Zhang J, Zhang C. Pim-3 enhances melanoma cell migration and invasion by promoting STAT3 phosphorylation. Cancer Biol Ther. 2018;19(3):160–8.
44. Liu YL, Ge FL, Zhu JX, Jing J, Wang JB, Zhang YM, Guo YM, Xiao XH. Re-evaluation of liver injury associated with Buguzhi Preparations based on passive monitoring data and hospital cases. Zhongguo Zhong Yao Za Zhi. 2019;44(19):4272–6.
45. Love MI, Huber W, Anders S. Moderated estimation of fold change and dispersion for RNA-seq data with DESeq2. Genome Biol. 2014;15(12):550.
46. Lu Y, Shao M, Xiang H, Zheng P, Wu T, Ji G. Integrative transcriptomics and metabolomics explore the mechanism of kaempferol on improving nonalcoholic steatohepatitis. Food Funct. 2020;11(11):10058–69.
47. McNeely W, Goa KL. 5-Methoxypsoralen. A review of its effects in psoriasis and vitiligo. Drugs. 1998;56(4):667–90.
48. Nam SW, Baek JT, Lee DS, Kang SB, Ahn BM, Chung KW. A case of acute cholestatic hepatitis associated with the seeds of Psoralea corylifolia (Boh-Gol-Zhee). Clin Toxicol (Phila). 2005;43(6):589–91.
49. Nesbitt NM, Malone LE, Liu Z, Jares A, Gnatenko DV, Ma Y, Zhu W, Bahou WF. Divergent erythroid megakaryocyte fates in Blvrb-deficient mice establish non-overlapping cytoprotective functions during stress hematopoiesis. Free Radic Biol Med. 2021;164:164–74.
50. Platten M, Nollen EAA, Röhrig UF, Fallarino F, Opitz CA. Tryptophan metabolism as a common therapeutic target in cancer, neurodegeneration and beyond. Nat Rev Drug Discov. 2019;18(5):379–401.
51. Qu Y, Zhang C, Du E, Wang A, Yang Y, Guo J, Wang A, Zhang Z, Xu Y. Pim-3 is a Critical Risk Factor in Development and Prognosis of Prostate Cancer. Med Sci Monit. 2016;22:4254–60.

52. Ren S, Shao Y, Zhao X, Hong CS, Wang F, Lu X, Li J, Ye G, Yan M, Zhuang Z, Xu C, Xu G, Sun Y. Integration of Metabolomics and Transcriptomics Reveals Major Metabolic Pathways and Potential Biomarker Involved in Prostate Cancer. Mol Cell Proteomics. 2016;15(1):154–63.
53. Sansaloni-Pastor S, Varesio E, Lange N. Modulation and proteomic changes on the heme pathway following treatment with 5-aminolevulinic acid. J Photochem Photobiol B. 2022;233:112484.
54. Sasabe N, Keyamura Y, Obama T, Inoue N, Masuko Y, Igarashi Y, Aiuchi T, Kato R, Yamaguchi T, Kuwata H, Iwamoto S, Miyazaki A, Hara S, Yoshikawa T, Itabe H. Time course-changes in phosphatidylcholine profile during oxidative modification of low-density lipoprotein. Lipids Health Dis. 2014;13:48.
55. Shen B, Kwan HY, Ma X, Wong CO, Du J, Huang Y, Yao X. cAMP activates TRPC6 channels via the phosphatidylinositol 3-kinase (PI3K)-protein kinase B (PKB)-mitogen-activated protein kinase kinase (MEK)-ERK1/2 signaling pathway. J Biol Chem. 2011;286(22):19439–45.
56. Shen T, Liu Y, Shang J, Xie Q, Li J, Yan M, Xu J, Niu J, Liu J, Watkins PB, Aithal GP, Andrade RJ, Dou X, Yao L, Lv F, Wang Q, Li Y, Zhou X, Zhang Y, Zong P, Wan B, Zou Z, Yang D, Nie Y, Li D, Wang Y, Han X, Zhuang H, Mao Y, Chen C. Incidence and Etiology of Drug-Induced Liver Injury in Mainland China. Gastroenterology. 2019;156(8):2230–41.e2211.
57. Spector AA, Gordon JA, Moore SA. Hydroxyeicosatetraenoic acids (HETEs). Prog Lipid Res. 1988;27(4):271–323.
58. Tsuge K, Inazumi T, Shimamoto A, Sugimoto Y. Molecular mechanisms underlying prostaglandin E2-exacerbated inflammation and immune diseases. Int Immunol. 2019;31(9):597–606.
59. van der Veen JN, Kennelly JP, Wan S, Vance JE, Vance DE, Jacobs RL. The critical role of phosphatidylcholine and phosphatidylethanolamine metabolism in health and disease. Biochim Biophys Acta Biomembr Biomembranes. 2017;1859(9 Pt B):1558–72.
60. Wang L, Wang Y, Wee A, Soon G, Gouw ASH, Yang R, Tian Q, Liu L, Ma H, Zhao X. Clinicopathological features of Bu Gu Zhi-induced liver injury, a long-term follow-up cohort study. Liver Int. 2020;40(3):571–80.
61. Wang P, Sun H, Lv H, Sun W, Yuan Y, Han Y, Wang D, Zhang A, Wang X. Thyroxine and reserpine-induced changes in metabolic profiles of rat urine and the therapeutic effect of Liu Wei Di Huang Wan detected by UPLC-HDMS. J Pharm Biomed Anal. 2010;53(3):631–45.
62. Wang S, Sui S, Liu Z, Peng C, Liu J, Luo D, Fan X, Liu C, Lu WY. Protective roles of hepatic gamma-aminobutyric acid signaling in acute ethanol exposure-induced liver injury. J Appl Toxicol. 2018;38(3):341–50.
63. Wang X, Du Y, Wu C, Xu M, Liu Y, Di X. UHPLC-MS/MS analysis of cAMP and cGMP in rat plasma as potential biomarkers of Yin-Yang disharmony in traditional Chinese medicine. J Pharm Anal. 2021;11(4):458–64.
64. Wang Y, Liu C, Hu L. Cholesterol regulates cell proliferation and apoptosis of colorectal cancer by modulating miR-33a-PIM3 pathway. Biochem Biophys Res Commun. 2019;511(3):685–92.
65. Wang Y, Liu H, McKenzie G, Witting PK, Stasch JP, Hahn M, Changsirivathanathamrong D, Wu BJ, Ball HJ, Thomas SR, Kapoor V, Celermajer DS, Mellor AL, Keaney JF Jr, Hunt NH, Stocker R. Kynurenine is an endothelium-derived relaxing factor produced during inflammation. Nat Med. 2010;16(3):279–85.

66. Watchko JF, Tiribelli C. Bilirubin-induced neurologic damage–mechanisms and management approaches. N Engl J Med. 2013;369(21):2021–30.
67. Wegiel B, Gallo D, Csizmadia E, Roger T, Kaczmarek E, Harris C, Zuckerbraun BS, Otterbein LE. Biliverdin inhibits Toll-like receptor-4 (TLR4) expression through nitric oxide-dependent nuclear translocation of biliverdin reductase. Proc Natl Acad Sci U S A. 2011;108(46):18849–54.
68. Wei SM, Yan ZZ, Zhou J. Psoralea corylifolia protects against testicular torsion/detorsion-induced ischemia/reperfusion injury. J Ethnopharmacol. 2011;137(1):568–74.
69. Wu C, Sun Z, Ye Y, Han X, Song X, Liu S. Psoralen inhibits bone metastasis of breast cancer in mice. Fitoterapia. 2013;91:205–10.
70. Wu S, Li Z, Gnatenko DV, Zhang B, Zhao L, Malone LE, Markova N, Mantle TJ, Nesbitt NM, Bahou WF. BLVRB redox mutation defines heme degradation in a metabolic pathway of enhanced thrombopoiesis in humans. Blood. 2016;128(5):699–709.
71. Xu Y, Zhao Y, Xie J, Sheng X, Li Y, Zhang Y. 2017. The Evaluation of Toxicity Induced by Psoraleae Fructus in Rats Using Untargeted Metabonomic Method Based on UPLC-Q-TOF/MS. Evid Based Complement Alternat Med 2017, 6207183.
72. Yang H, Xing R, Liu S, Yu H, Li P. Rescuing fluoride-induced damages in liver with gamma aminobutyric acid. Biochem Biophys Res Commun. 2017;491(1):19–24.
73. Yu B, Wang AH, Zhou K, Chai LJ, Liu L. Molecular Pathway of Psoralidin-Induced Apoptosis in HepG2 Cell Line. Chin J Integr Med. 2019;25(10):757–62.
74. Zhang C, Zhao JQ, Sun JX, Li HJ. Psoralen and isopsoralen from Psoraleae Fructus aroused hepatotoxicity via induction of aryl hydrocarbon receptor-mediated CYP1A2 expression. J Ethnopharmacol. 2022;297:115577.
75. Zhang L, Niu M, Wei AW, Tang JF, Tu C, Bai ZF, Zou ZS, Xiao XH, Liu YP, Wang JB. Risk profiling using metabolomic characteristics for susceptible individuals of drug-induced liver injury caused by Polygonum multiflorum. Arch Toxicol. 2020;94(1):245–56.
76. Zhang X, Zhao W, Wang Y, Lu J, Chen X. The Chemical Constituents and Bioactivities of Psoralea corylifolia Linn.: A Review. Am J Chin Med. 2016;44(1):35–60.
77. Zhang XJ, Cheng X, Yan ZZ, Fang J, Wang X, Wang W, Liu ZY, Shen LJ, Zhang P, Wang PX, Liao R, Ji YX, Wang JY, Tian S, Zhu XY, Zhang Y, Tian RF, Wang L, Ma XL, Huang Z, She ZG, Li H. An ALOX12-12-HETE-GPR31 signaling axis is a key mediator of hepatic ischemia-reperfusion injury. Nat Med. 2018;24(1):73–83.
78. Zhang Y, Xu SY, Liu MN, Jia TY, Qu WJ, Han T, Jia Z, Xu XF, Li XR. 2019. Comparative Studies on Chemical Contents and Effect in Kidney-Yang Deficiency Rats of Salt-Processed Product and Wine-Processed Product of Cuscutae Semen. Evid Based Complement Alternat Med 2019, 2049497.
79. Zhou Z, Zhang R, Wang R, Zhang Y, Xu L, Chen J, Zhang J, Huang Z, Chen M, Pan Z. Expression of Pim-3 in colorectal cancer and its relationship with prognosis. Tumour Biol. 2016;37(7):9151–6.

Figures

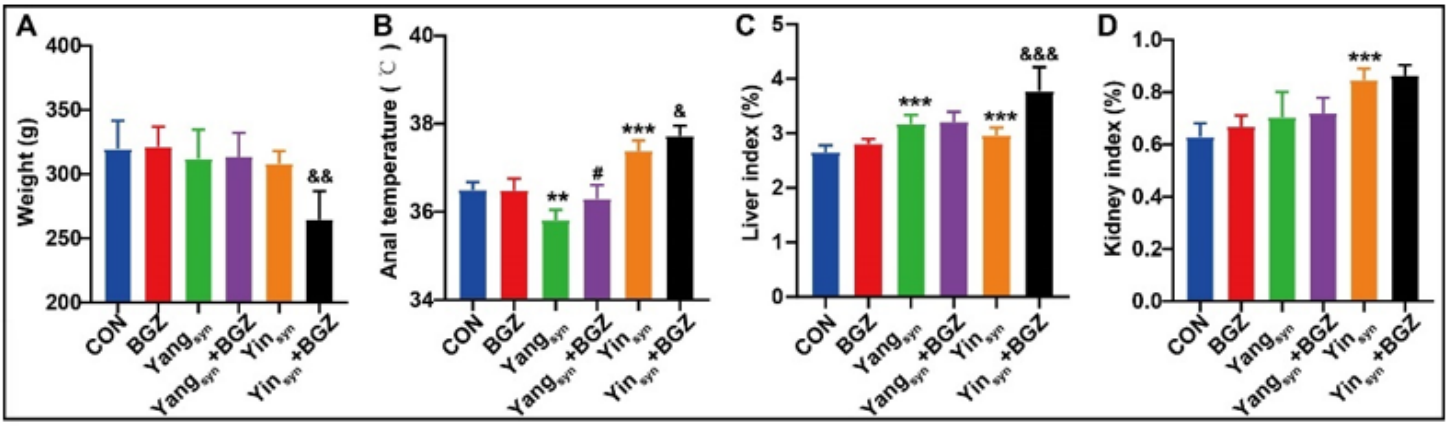


Figure 1

Effect of BGZ treatment on changes in body weight, anal temperature, and organ indexes (N=8). Weight (A), anal temperature (B), liver index (C), and kidney index (D). **P < 0.05, **P < 0.01, ***P < 0.001*, compared with CON group; *$^{\#}$P < 0.05,* compared with Yang$_{syn}$ group; *$^{\&}$P < 0.05*, *$^{\&\&}$P < 0.01*, *$^{\&\&\&}$P < 0.001*, compared with Yin$_{syn}$ group.

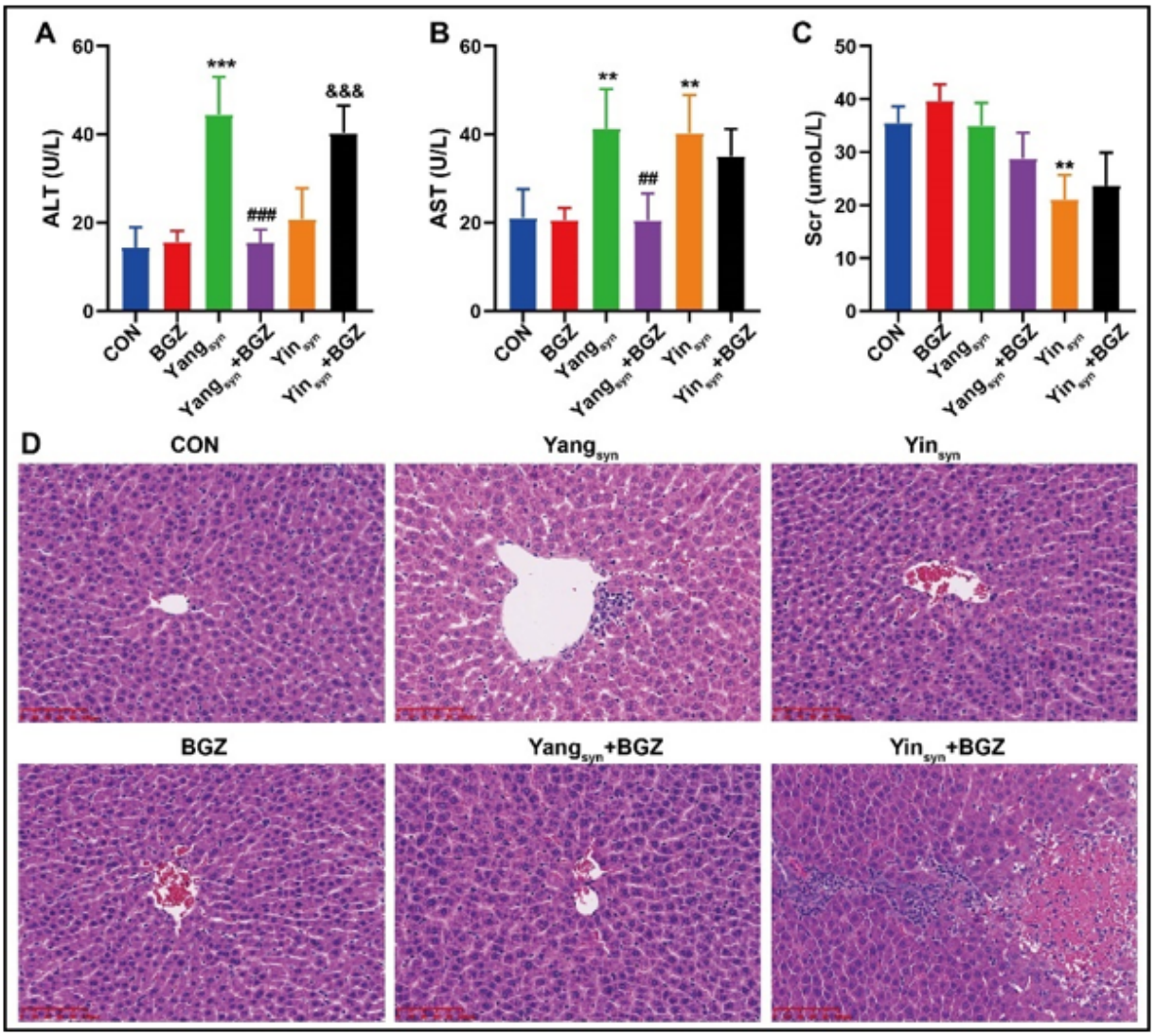


Figure 2

Effect of BGZ treatment on serum biochemistry and histopathological examination (N=6~8). Serum ALT (A), AST (B), and SCr (C) activity. ***P < 0.01*, ****P < 0.001*, compared with CON group; *##P < 0.01, ###P < 0.001*, compared with $Yang_{syn}$ group; *&&&P < 0.001*, compared with Yin_{syn} group. (D) Typical histopathological section photographs of rat liver specimens for HE analysis (Scale bar, 100 μm).

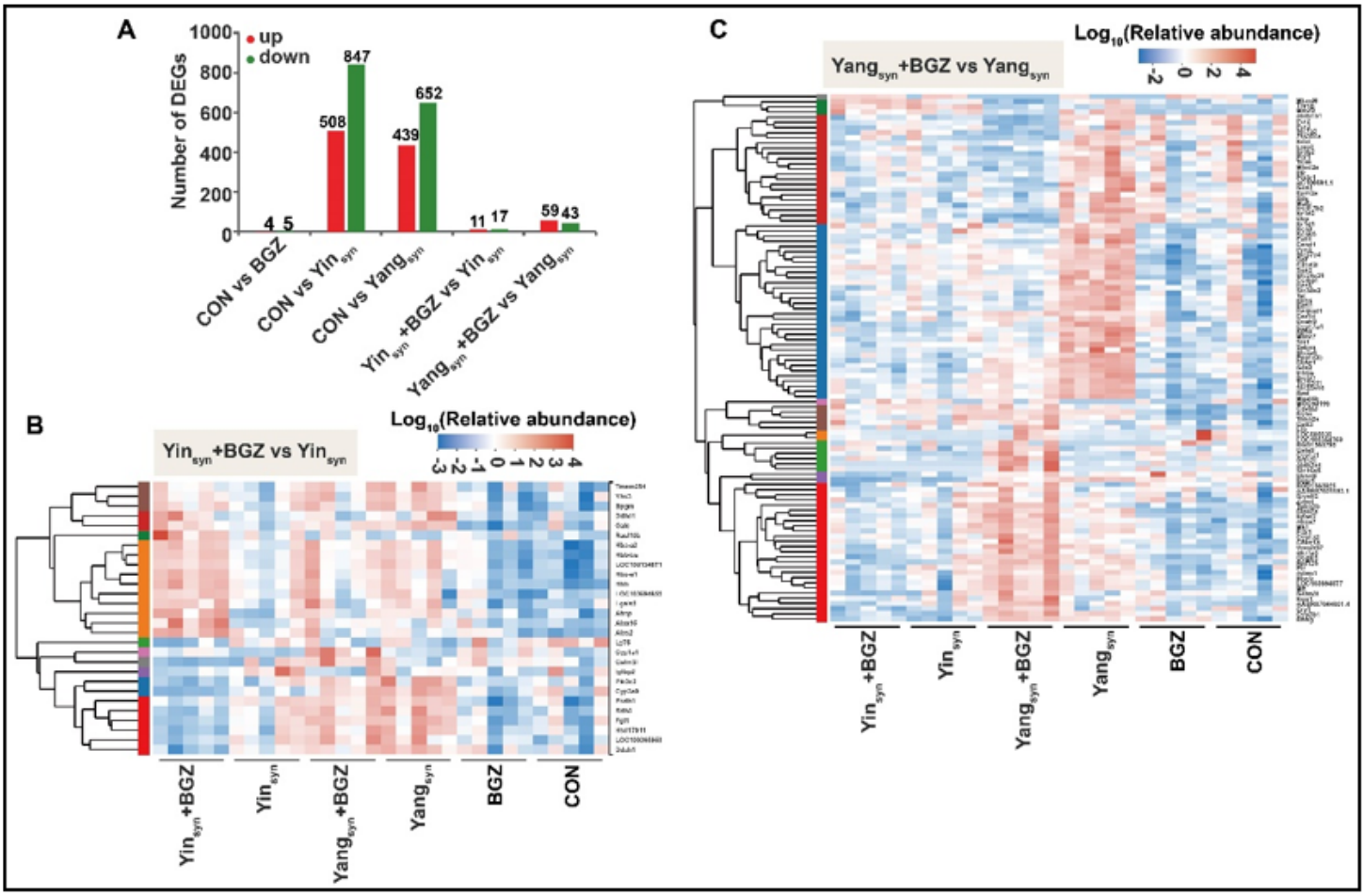


Figure 3

Transcriptomic alterations of BGZ treatment on Yin_{syn} and $Yang_{syn}$ rats (N=5). (A) The number of DEGs compared with each group. The red color represents up-regulated genes and the green color represents down-regulated genes. (B) Heatmap showing the intersection of DEGs between the Yin_{syn}+BGZ group and the Yin_{syn} group. (C) Heatmap showing the intersection of DEGs between the $Yang_{syn}$+BGZ group and the $Yang_{syn}$ group. DEGs: differentially expressed genes.

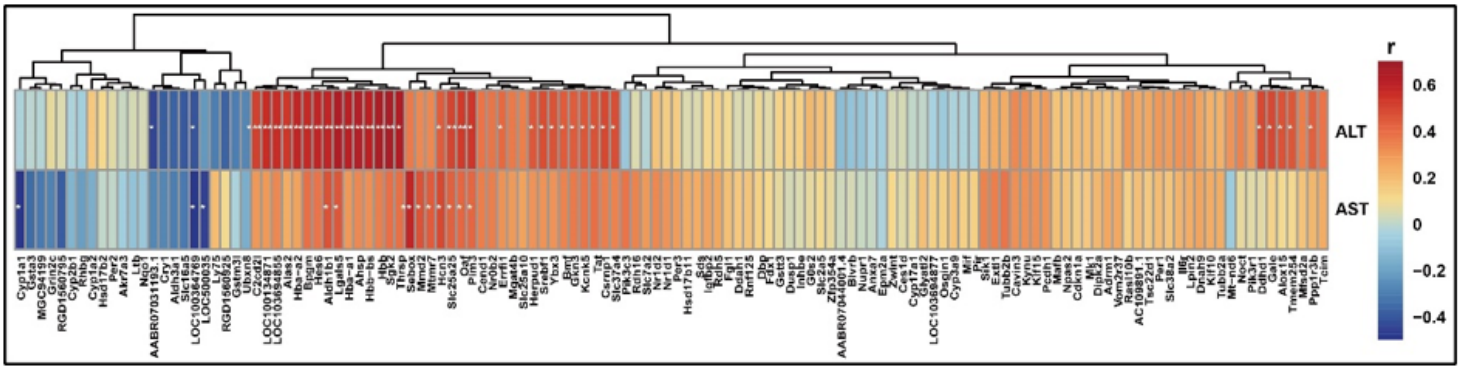


Figure 4

The relationship between DEGs and the levels of serum biochemistry (ALT and AST). (A) Heatmap of correlation between the levels of serum biochemistry (ALT and AST) and DEGs (N=5). Color depth represents correlation strength, the red color represents positive correlation, and the blue color represents negative correlation. **P < 0.05*, ***P < 0.01*, ****P < 0.001*.

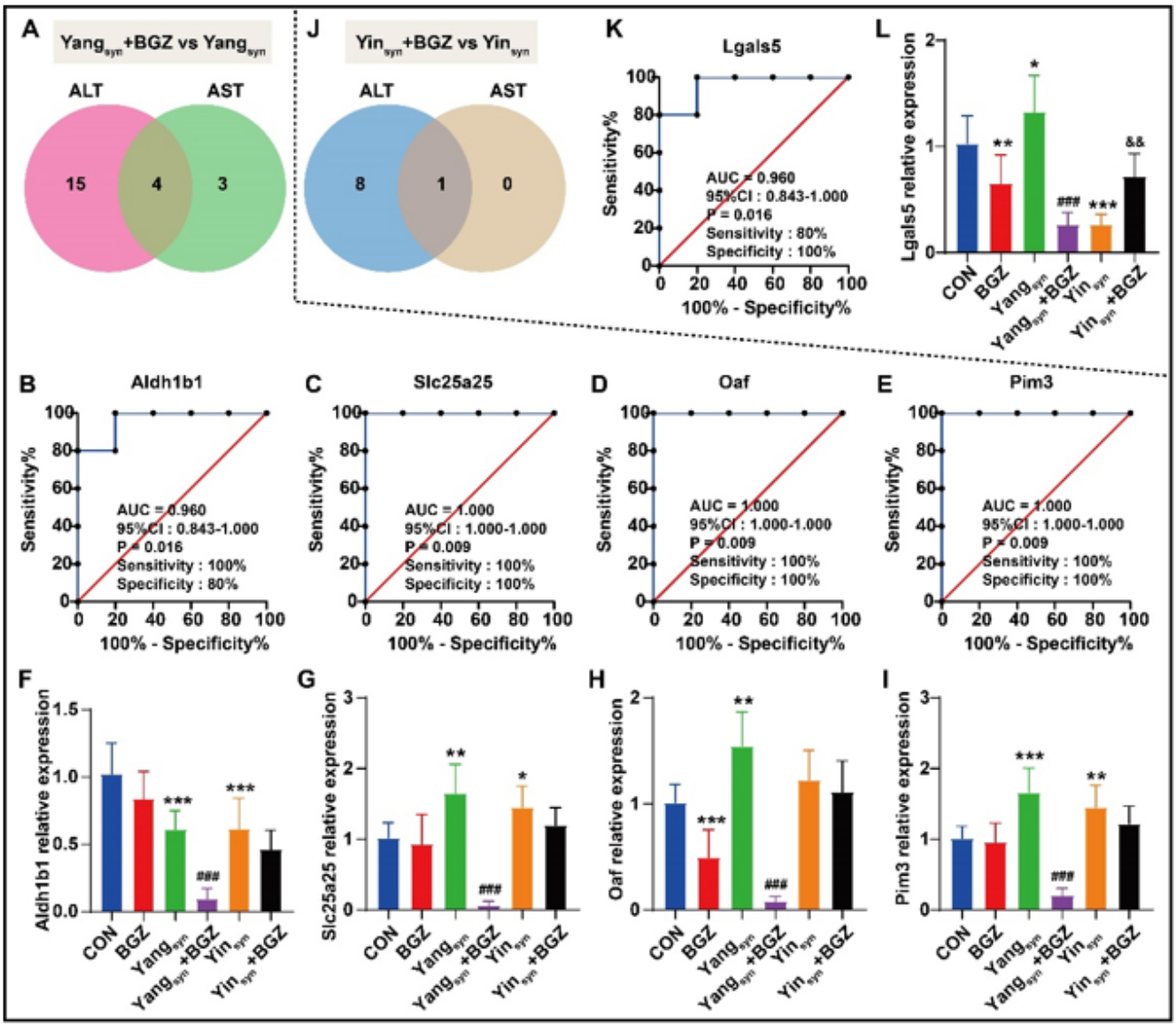


Figure 5

ROC analysis of DEGs associated with ALT and AST expression and RT-qPCR verification. (A) Venn diagram showing the number of DEGs associated with the levels of ALT and AST under ROC > 0.90 between the $Yang_{syn}$+BGZ group and the $Yang_{syn}$ group. (B-E) ROC curves of DEGs associated with the levels of ALT and AST under ROC > 0.90 between the $Yang_{syn}$+BGZ group and $Yang_{syn}$ group, Aldh1b1 (B), Slc25a25 (C), Oaf (D), and Pim3 (E). (J) Venn diagram showing the number of DEGs associated with the levels of ALT and AST under ROC > 0.90 between the Yin_{syn}+BGZ group and the Yin_{syn} group. (K) ROC curves of Lgals5 between the Yin_{syn}+BGZ group and the Yin_{syn} group. (F-I and L) The mRNA expression of Aldh1b1 (F), Slc25a25 (G), Oaf (H), Pim3 (I), and Lgals5 (L). *$^{*}P < 0.05$, $^{**}P < 0.01$, $^{***}P < 0.001$*, compared with CON group; *$^{\#\#\#}P < 0.001$*, compared with $Yang_{syn}$ group; *$^{\&\&}P < 0.01$*, compared with Yin_{syn} group. DEGs: differentially expressed genes; ROC: receptor operating characteristic; AUC: area under the ROC curve; CI: confidence interval.

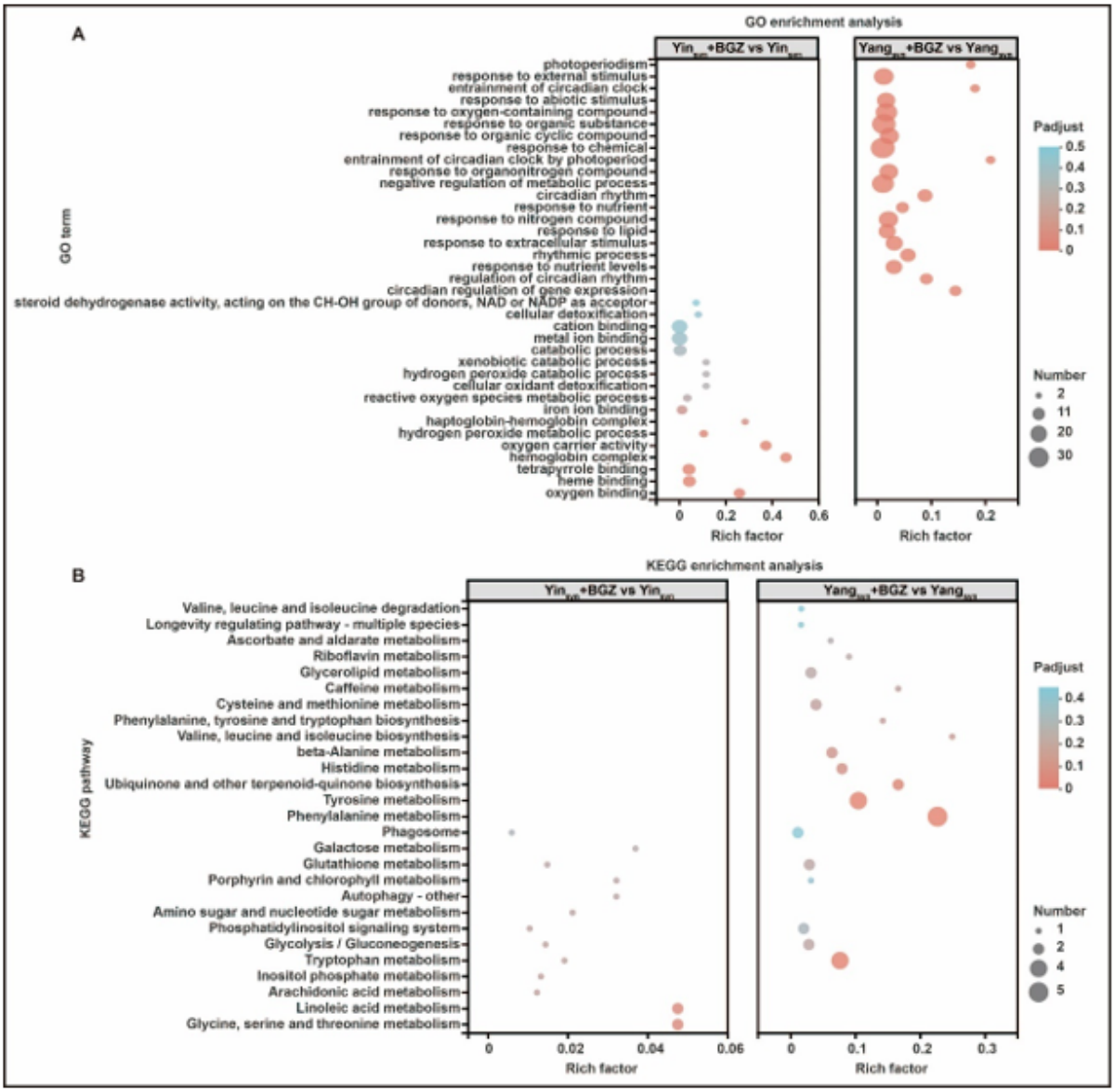


Figure 6

GO and KEGG functional enrichment pathways analysis of DEGs. (A) GO enrichment analysis. (B) KEGG enrichment analysis. DEGs: differentially expressed genes; GO: Gene Ontology; KEGG: Kyoto Encyclopedia of Genes and Genomes.

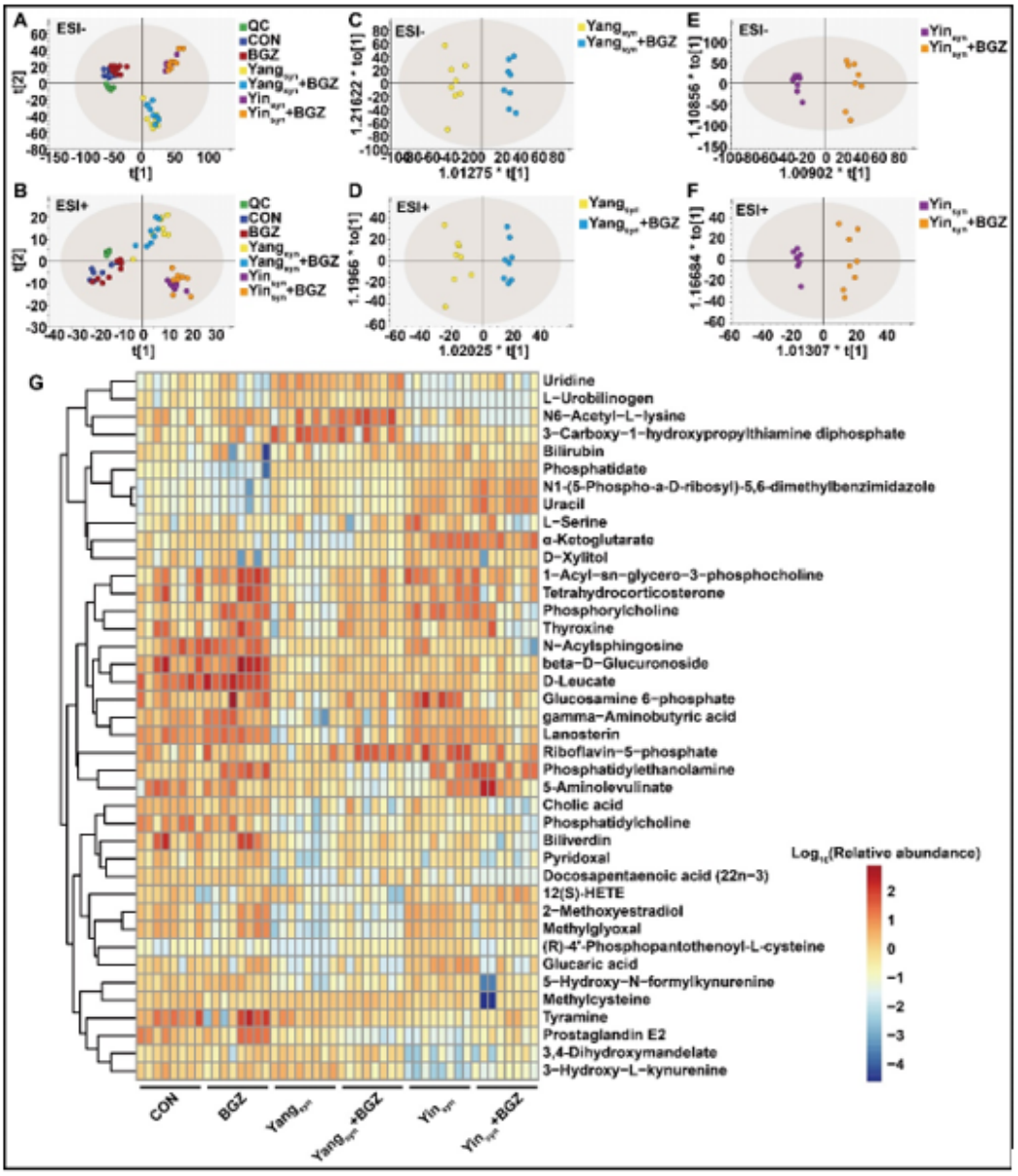


Figure 7

Metabolomic alterations of BGZ treatment on Yin_{syn} and $Yang_{syn}$ rats (N=8). (A-B) Scatter plot of liver metabolites in all groups determined by PCA in ESI- mode (A) and ESI+ mode (B). (C-D) Scatter plot of liver metabolites between the $Yang_{syn}$+BGZ and $Yang_{syn}$ groups determined by OPLS-DA in ESI- mode (C) and ESI+ mode (D). (E-F) Scatter plot of liver metabolites between the Yin_{syn}+BGZ and Yin_{syn} groups determined by OPLS-DA in ESI- mode (E) and ESI+ mode (F). (G) Heatmap of the metabolites identified. Color depth represents the variation trend of the relative abundance of metabolites, the red color represents up-regulated

metabolites, and the blue color represents down-regulated metabolites. ESI+: electrospray ionization source positive; ESI-: electrospray ionization source negative; PCA: Principal Component Analysis; OPLS-DA: Orthogonal Projections to Latent Structures Discriminant Analysis.

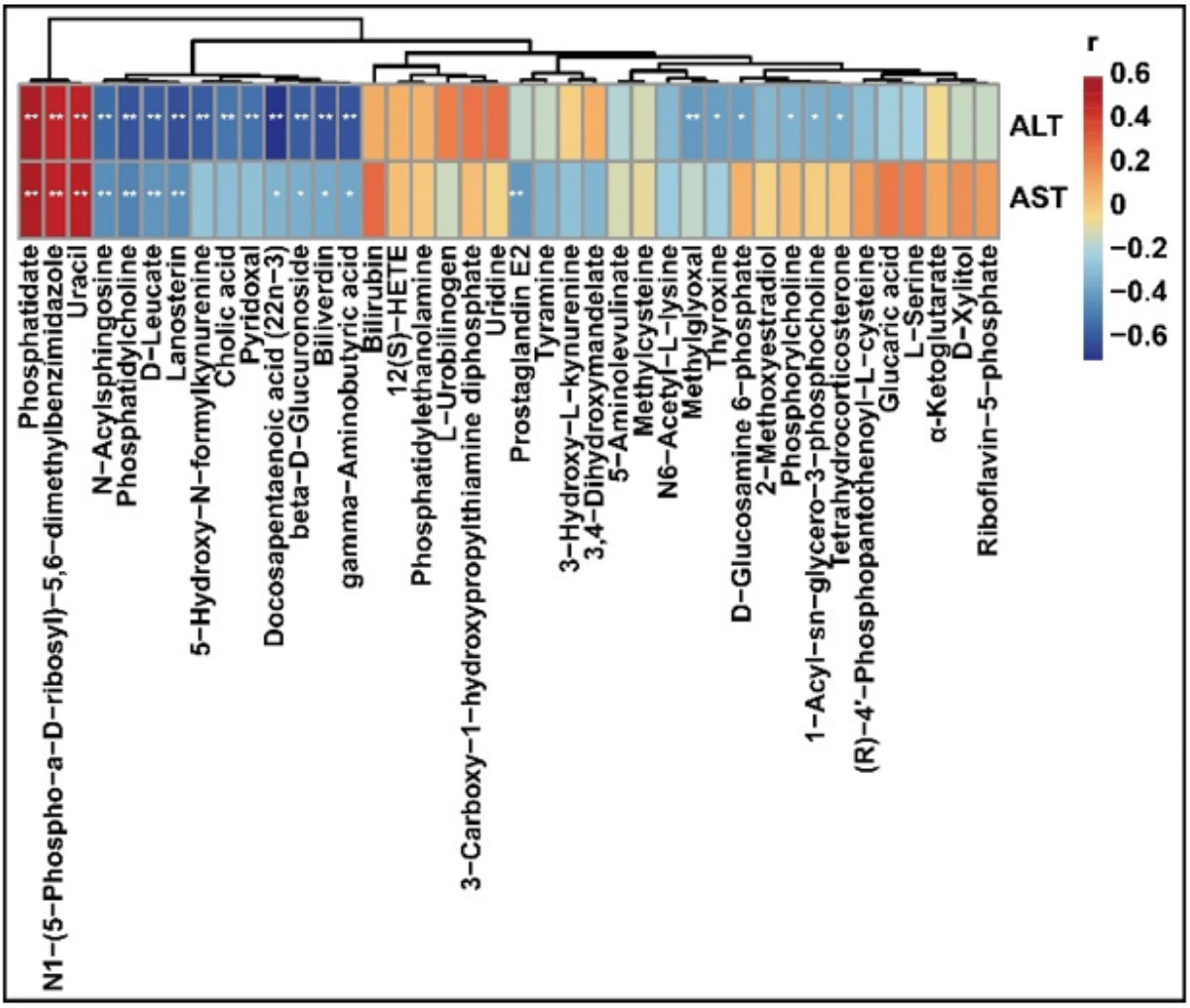


Figure 8

Heatmap of correlation between serum biochemistry (ALT and AST) and metabolites (N=6~8). The color depth represents correlation strength, the red color represents positive correlation, and the blue color represents negative correlation. **P < 0.05*, ***P < 0.01*, ****P < 0.001*.

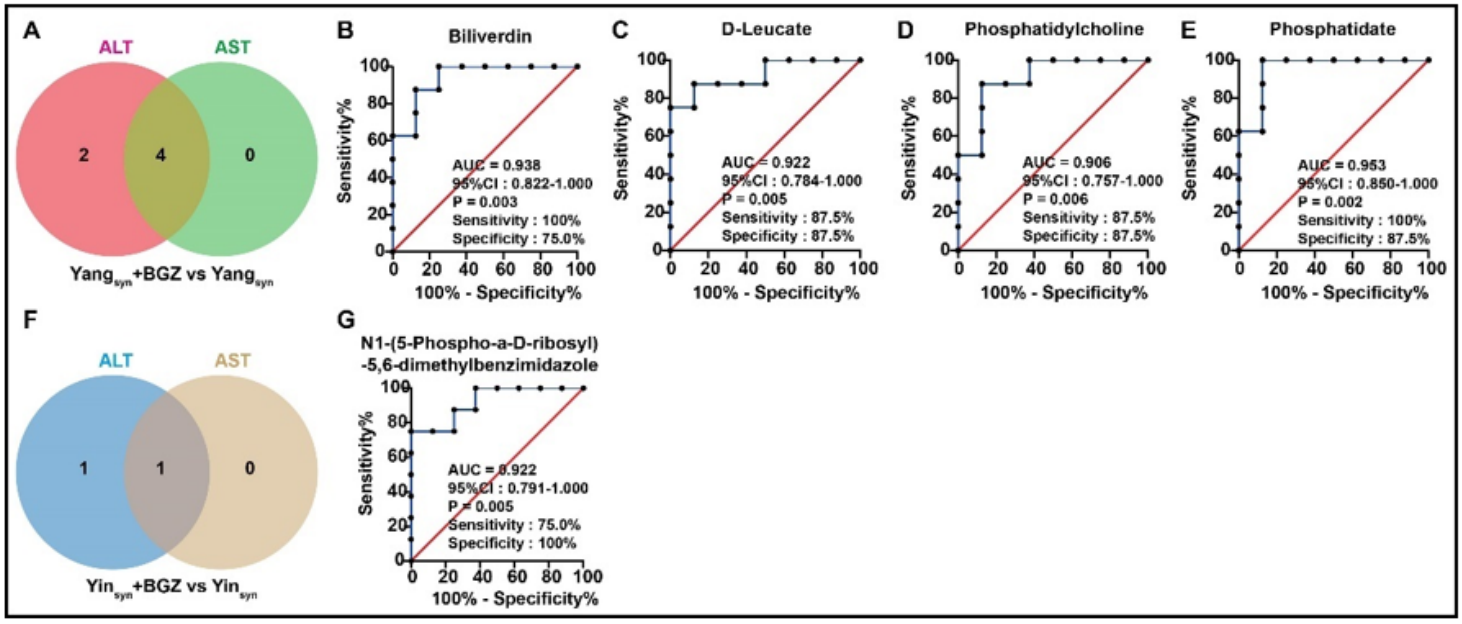


Figure 9

ROC analysis of metabolites associated with ALT and AST expression (N=8). (A) Venn diagram showing the number of metabolites associated with the levels of ALT and AST under ROC > 0.90 between the Yang$_{syn}$+BGZ group and the Yang$_{syn}$ group. (B-E) ROC curves of metabolites associated with the levels of ALT and AST under ROC > 0.90 between the Yang$_{syn}$+BGZ group and the Yang$_{syn}$ group. Biliverdin (B), D-Leucate (C), Phosphatidylcholine (D), Phosphatidate (E). (F) Venn diagram showing the number of metabolites associated with the levels of ALT and AST under ROC > 0.90 between the Yin$_{syn}$+BGZ group and the Yin$_{syn}$ group. (G) ROC curves of N1-(5-Phospho-a-D-ribosyl)-5,6-dimethylbenzimidazole between the Yin$_{syn}$+BGZ group and the Yin$_{syn}$ group. ROC: receiver operating characteristic, AUC: area under the ROC curve, CI: confidence interval.

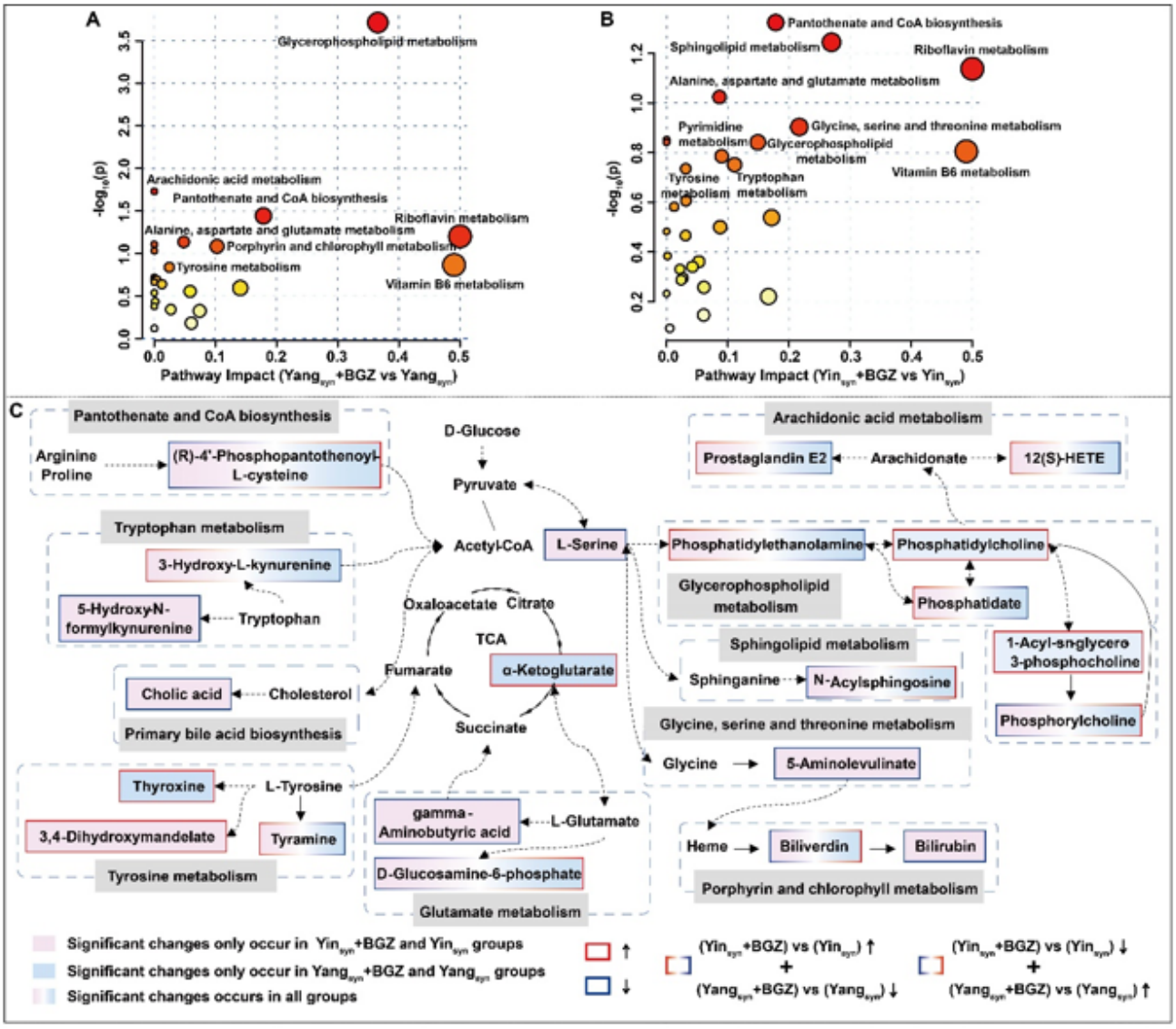


Figure 10

Overall metabolic profile. (A and B) Schematic diagram of the disturbed metabolic pathways for the BGZ treatment on $Yang_{syn}$ (A) and Yin_{syn} (B) rats. (C) Correlation network diagram of DEGs and metabolism of BGZ intervention in Yin_{syn} and $Yang_{syn}$ rats.

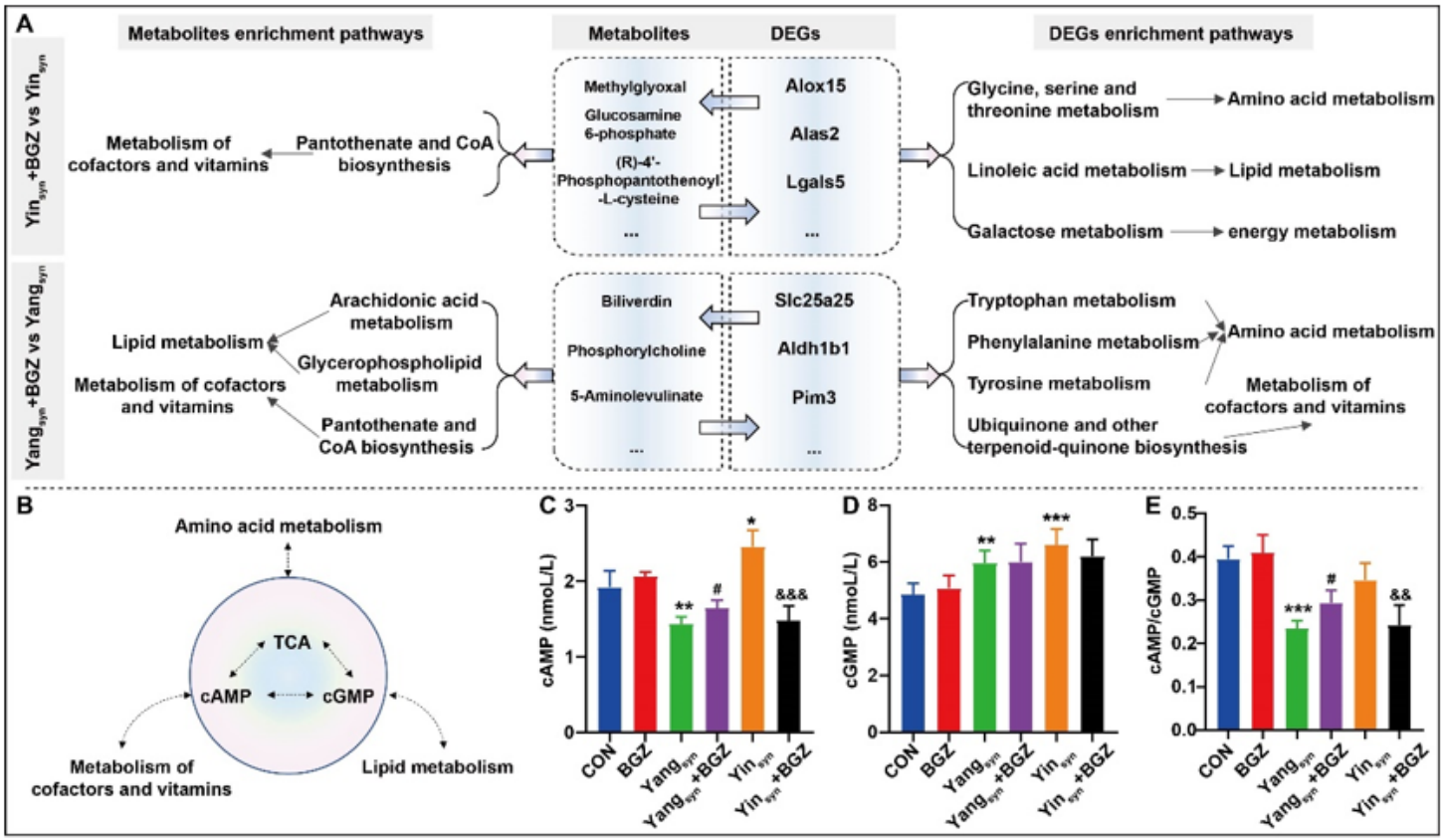


Figure 11

Integration analysis of metabolite and DEGs enrichment pathway. (A) Pathways of co-regulation of metabolites and (or) DEGs by BGZ in Yin_{syn} and $Yang_{syn}$ rats, (B) Schematic diagram of the relationship between cAMP and cGMP and the pathway of BGZ regulating Yin_{syn} and $Yang_{syn}$. pathways of co-regulation or specific regulation of metabolites and DEGs by BGZ in Yin_{syn} and $Yang_{syn}$ rats. Effect of BGZ treatment on the changes in the expression of cAMP (C), cGMP (D), and the ratio of cAMP/cGMP (E) (N=6~8). *$^{*}P < 0.05$, $^{**}P < 0.01$, $^{***}P < 0.001$*, compared with CON group; *$^{\#}P < 0.05$,* compared with $Yang_{syn}$ group; *$^{\&\&}P < 0.01$, $^{\&\&\&}P < 0.001$*, compared with Yin_{syn} group. DEGs: differentially expressed genes; cAMP: cyclic adenosine monophosphate; cGMP: cyclic guanosine monophosphate; TCA: tricarboxylic acid cycle.

Supplementary Files

This is a list of supplementary files associated with this preprint. Click to download.

- SupplementaryTablesandFigures.docx